Analysis of the Effect of Glaziovianin A and the Derivatives on Microtubule Dynamics

September 2014

Takumi CHINEN

Analysis of the Effect of Glaziovianin A and the Derivatives on Microtubule Dynamics

A Dissertation Submitted to

the Graduate School of Life and Environmental Sciences,

the University of Tsukuba

in Partial Fulfillment of the Requirements

for the Degree of Doctor of Philosophy in Agricultural Science

(Doctoral Program in Life Sciences and Bioengineering)

Takumi CHINEN

Contents

Analysis of the effect of glaziovianin A and the derivatives on microtubule dynamics.

CHAPTER 1. Introduction

Microtubules, a component of the cytoskeleton in eukaryotes, have a cylindrical structure that consists of polymerized α/β-tubulin. Microtubules are involved in spindle formation in mitosis, cellular signaling, cell motility and the determination of organelle positions.

In mitosis, there is a key regulation machinery, mitotic/spindle checkpoint which regulate the entry to anaphase. In this checkpoint system, the kinetochore in the prophase/early prometaphase recruits several mitotic checkpoint components, (e. g. BUBR1, MAD2, CEMPE and more), which inhibit the CDC20-dependent recognition of cyclin B and securin by Anaphase promoting complex/Cyclosome (APC/C). When the microtubules are captured and tension is detected at the kinetochore, the mitotic checkpoint is satisfied, and the cell cycle progresses with entries into anaphase by the degradation of cyclin B and securin by APC/C.[1] But when even one chromosome is not properly captured by microtubules, the mitotic checkpoint is activated to keep cells from aneuploidy and apoptotic cell death. Because cancer cells have abnormal mitotic checkpoints, miss segregation and apoptosis are easily induced in cancer cells.[2]

Microtubule polymerization inhibitors (e.g., *vinca* alkaloids) and microtubule stabilizers (e.g., taxane) have been used for cancer chemotherapy. These microtubule inhibitors prevent spindle formation and arrest cell cycle progression at M-phase by activating the mitotic/spindle checkpoint, subsequently inducing cell death in cancer.[3] However, these microtubule inhibitors can also cause some severe side effects, including peripheral neuropathy. It is thought that this side effect occurs due to the extreme effects on the microtubules of non-proliferative cells, which are in interphase.[3]

Against this background, microtubule dynamics have been recognized as an attractive target for cancer chemotherapy that may help avoid the side effects of microtubule destabilizers and stabilizers. Microtubule plus ends repeatedly grow and then shorten, and this phenomenon is called "microtubule dynamics". These dynamics are regulated by GTP/GDP on β-tubulin.[4] In α-tubulin, GTP is not hydrolyzed and it supports the structure of tubulin heterodimer. In contrast, GTP bound to β-tubulin is hydrolyzed, and the hydrolysis reaction changes the conformation of the α/β-tubulin heterodimer, and subsequently the de-polymerization of microtubule occurs (this transition forward to de-polymerization is called a "catastrophe"). Microtubule dynamics consist of three phases, growing, shortening, and pause (neither growing nor shortening) and two transitions: catastrophe (transition from growing or pause to shortening) and rescue (transition from shortening to growing or pause).

For example, the microtubule dynamics inhibitor, eribulin, a synthetic analog of halicondrine

B,[5] is marketed by Esai Pharmaceutical Company and used to treat patients with metastatic breast cancer who have received at least two prior treatments in the EU,[6] U.S.[7] and Japan.[8] This compound binds to the plus end of microtubules and inhibits microtubule elongation but not shortening.[9,10] Another microtubule dynamics inhibitor, noscapin, is undergoing a phase I/II clinical trial for multiple myeloma.[3] These compounds have little effect on the microtubule network in interphase cells, but they induce abnormal spindle formation. Except for their interference with bipolar spindle formation, the effects of microtubule dynamics inhibitors on the cell functions have not been revealed. It is thus quite important to understand the functions of microtubule dynamics in cells to prevent the side effects induced by microtubule dynamics inhibitors.

Glaziovianin A (AG1, Fig. 1), a new isoflavone isolated from the leaves of Brazilian pea *Ateleia glazioviana*, induces abnormal spindle formation (an abnormal alignment of chromosomes and multi-polar spindles) and arrests cell cycle progression of mammalian cells at M-phase.[11] In a cancer cells panel screening performed by the Screening Committee for Anticancer Drugs (SCAD), AG1 showed similar score to those of microtubule polymerization inhibitors,[11] suggesting that AG1 is a microtubule polymerization inhibitor. In previous studies, the effects of AG1 was investigated on the microtubules and it was revealed that AG1 delayed tubulin polymerization *in vitro* (Fig. 2) and that the signals of EB1 (a microtubule plus end binding protein), which accumulates at growing microtubule plus ends,[12, 13] disappeared soon after AG1 treatment (Fig. 3). These data suggested that

AG1 directly binds tubulin heterodimer and attenuated microtubule polymerization, and probably de-polymerization as well. However, the details of the effects of AG1 on microtubules and its inhibitory mechanisms remain to be revealed. In this thesis, therefore, I investigated the binding site of AG1 on tubulin heterodimer and AG1's effect on microtubule dynamics *in vitro* and *in vivo*.

To analyze the mode of action of small molecules, not only mammalian cells[14,15] but also a model organism such as yeast[16,17] are often used. Mammalian cells are useful for analyses, such as observation of organelles using microscopy,[14,15], biochemical experiments,[15] because they are easy to observe their organelles morphology and to lyse the cells. In the field of chemical biology, mammalian cell's high sensitivities against small compounds facilitates the analyses of mode of action. However, analyses of microtubule inhibitors are sometimes difficult because human cells have approximately eight α- and eight β-tubulin isoforms. Tubulins function as heterodimer, the number of the combination of α- and β-tubulin isoforms would thus be more than 60. In addition, several posttranslational modifications of microtubules, such as acetylation, phosphorylation, polyglutamylation and polyglycylation, have been reported.[18] These complexity make analysis of microtubule inhibitors difficult.

The budding yeast *Saccharomyces cerevisiae,* is also a useful tool for chemical biology studies because it is easy to use genetic analyses, mutational analyses,[16] gene disruption, and genome modification[14,17,19] (Fig. 4). *S. cerevisiae* has only two α-tubulin genes (*TUB1* and *TUB3*)

and one ß-tubulin gene (*TUB2*), and *TUB3* gene can be disrupted.[20] *S. cerevisiae* can thus express

single allele of α-/β-tubulin isoform (Tub1p and Tub2p) and genetic modifications of these genes

are useful ways to analyze the mode of action of AG1 and other microtubule inhibitors.[21] However,

there is a major obstacle for mode of action analyses using *S. cerevisiae*. Budding yeast is resistant

to most of the compounds to which mammalian cells are sensitive (Table 1). Therefore, new strains

showing high sensitivities to AG1 are required for the analysis of the mode of action of AG1.

In our laboratory, the molecular targets or binding sites of several bioactive compounds were

determined using yeast genetics.[14,16,17] To determine the target molecules and/or the binding site, it

has been necessary to construct yeast strains suitable for the various compounds,[16,22,23] but the

construction of deletion strains that have sensitivities specific to each of the various compounds is a

time-consuming process. Hence I speculated that the deletion of all of these genes (except those that

are important for viability and genetic experiments) could increase the drug sensitivity without

influencing transformation, mating, or sporulation efficiency.

There are two factors conferring multidrug resistance in *S. cerevisiae*: one is the drug efflux

system, and other is the permeability barrier. The drug efflux system is composed of ATP-binding

cassette (ABC) transporters that export xenotoxic compounds to outside of cells or inside of

vacuole[24-26] and the transcriptional factors of ABC transporters.[25,26] *S. cerevisiae* has at least 16

ABC transporters, of which Pdr5p, Snq2p and Yor1p confer multidrug resistance by exporting

bioactive small molecules out of cells. And four transcriptional factors (Pdr1p, Pdr3p, Pdr8p and Yrr1p) up-regulate the transcription of most of the ABC transporters. In contrast, the major factor for the permeability barrier is ergosterol in the yeast plasma membrane. For these reasons, multidrug-sensitive strain lacking *PDR1*, *PDR3* (transcriptional factors for ABC transporters) and *ERG6* (ergosterol synthase) are used for drug screening.[27] However, this deletion mutant which lacks 3 genes (*pdr1*, *pdr3*, and *erg6*) decreases the transformation and sporulation efficiencies that are essential for yeast genetic analysis. I therefore hypothesized that it is possible to make highly multidrug-sensitive strain by the disruption of ABC transporters.

In this thesis I focused on ABC transporters on only the plasma membrane (including Pdr5p, Snq2p and Yor1p) and their transcription factors. The constructed strain lacking eight ABC transporters and four transcription factors showed sensitivity against several compounds, but they were not sensitive to AG1 or AG1 derivatives. I therefore next introduced the *ERG6* inducible expression system, and finally succeeded in constructing a strain showing sensitivity to AG1 derivative.
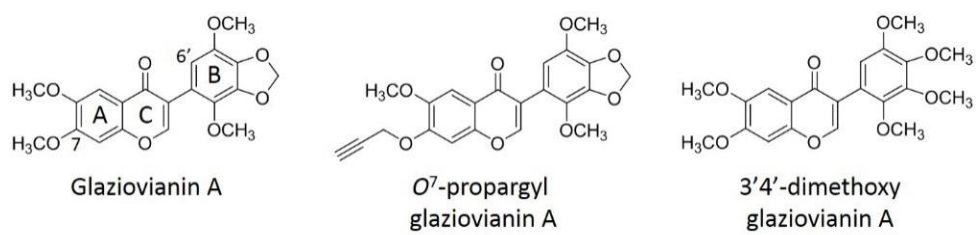
Fig. 1. The chemical structures of glaziovianin A (AG1) and its derivatives.
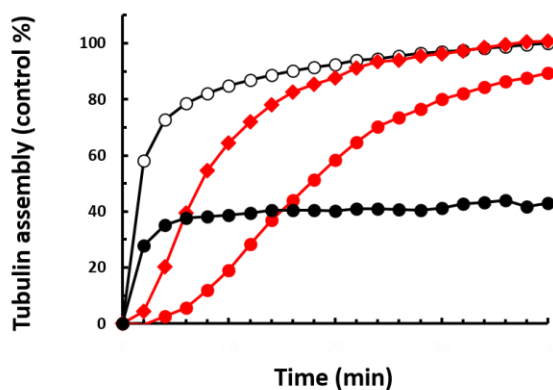
Fig. 2. AG1 inhibits tubulin polymerization *in vitro*.[15]

One mg/mL α/β-tubulin heterodimer purified from pig brain was mixed with each compounds. Tubulin polymerization was determined by measuring the absorbance at 350 nm. Black open and closed circles represent DMSO (control) and colchicine 10 µM, respectively. Red closed diamond and circle represent 10 and 15 µM AG1, respectively. Colchicine suppressed the total mass of polymerized tubulin, whereas AG1 delayed the α/β-tubulin polymerization in a dose-dependent manner.

EB1-Venus expressing HeLa cells
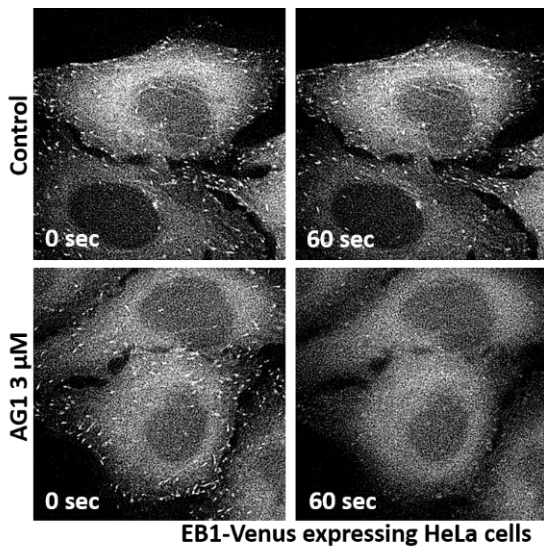
Fig. 3. AG1 suppressed the EB1 signal in cells.[15]

EB1, one of the plus‑end tracking proteins (+TIPs), accumulates at the plus end of growing microtubules. EB1-Venus-expressing HeLa cells were treated with AG1. The EB1 signal was drastically decreased within 1 min after the AG1 treatment, suggested that AG1 suppressed the microtubule dynamics in the cells.[15]
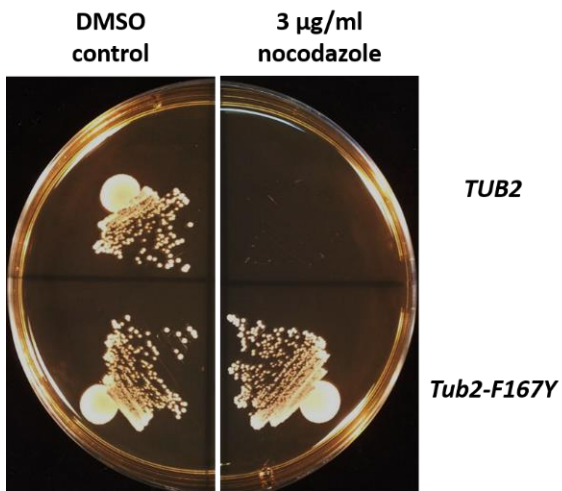
Fig. 4. Genetic modification for analysis of drug-target interactions.[19]

F167Y mutation in TUB2, β-tubulin gene in *S. cerevisiae*, showed microtubule depolymerizer nocodazole resistance. The left plate contained DMSO (control) and the right plate contained 3 μg/mL nocodazole.

	IC$_{50}$ value	
	HeLa cells	BY4741
Cycloheximide (μM)	0.2	270.0
Digitonin (μM)	0.4	1.9
Fluphenazine (μM)	13.0	51.0
Latrunculin A (nM)	0.2	>240.0
4-NQO (μM)	0.1	7.1
Staurosporine (μM)	0.1	15.1
Tunicamycin (μM)	1.8	>120.0

Table 1. Drug sensitivities of HeLa cells and *S. cerevisiae*, BY4741.

I compared IC$_{50}$ values of several compounds to HeLa cells and BY4741 by WST-8 assay.

CHAPTER 2. Analysis of the effect of glaziovianin A and the derivatives on microtubule dynamics

1. Summary

This chapter describes the analysis of the effects of AG1 on tubulin *in vitro* and in mammalian cells. The results of *in vitro* analysis suggested that the binding site of AG1 is close to the colchicine binding site on the tubulin heterodimer. A detailed time-lapse analysis revealed that AG1 decreased not only both of the speeds of the growing and the shortening of microtubules, but also the frequency of catastrophes, resulting in an increase of microtubules in the pause state. These finding clearly indicated that AG1 is a microtubule dynamics inhibitor and can be used as a "Bioprobe" for investigations of microtubule dynamics in cells. I therefore investigated the functions of microtubule dynamics on endocytosis using AG1, and found that AG1 inhibited both the proper transport of epidermal growth factor (EGF)-stimulated epidermal growth factor receptor (EGFR), and the EGFR signal down-regulation that is normally observed during the transport of the endosome. These results suggested that AG1 prevents endosome transport and maturation. In addition, EGF stimulated the cell death of AG1-pretreated A431 cells, an EGFR-overexpressing cell line, in a dose-dependent manner, indicating that microtubule dynamics are required for the function of endosome regulation and that microtubule dynamics inhibitors induce cell death by two

pathways, the inhibition of bipolar spindle formation, and endosome maturation.

2. Introduction

As mentioned in Chapter 1, microtubule dynamics have been recognized as an attractive drug target for cancer chemotherapy, but the details of the functions of microtubule dynamics in cellular process are unclear. It is thus worthwhile to reveal the *in situ* and *in vivo* functions of microtubule dynamics.

The effect of AG1 on the microtubules were investigated in previous studies, revealing that AG1 delays tubulin polymerization *in vitro* (Fig. 2) and that EB1 signals, which accumulates at growing microtubule plus ends,[12,13] disappeared soon after AG1 treatment (Fig. 3). These results suggested that AG1 inhibits microtubule dynamics by attenuating microtubule polymerization and probably de-polymerization. However, there is no direct information about the effect of AG1 on microtubule dynamics, especially about shortening phase. The elucidation of the direct effects of AG1 on microtubule dynamics in cells is an important question to be revealed.

There are two major binding sites of tubulin polymerization inhibitors, colchicine[28] and the *vinca* alkaloid site[29] (Fig. 5). AG1 is thought to bind at one of these binding sites on tubulin heterodimer, because AG1 delays (inhibits) tubulin polymerization *in vitro*. In addition, it is possible to analyze microtubule dynamics in cells by observing the movement of EGFP-α-tubulin. In this chapter, the analysis of the AG1 binding site and microtubule dynamics in AG1-treated cells is described, and demonstrate that AG1 binds to the colchicine binding site and inhibits microtubule

dynamics. These results strongly suggest that AG1 is a valuable tool for investigating microtubule dynamics in cells.

One possible function of microtubule dynamics is in endocytosis. It was reported that EB1 binds Gapex-5 (a guanine nucleotide exchange factor [GEF] for Rab5) and is involved in phagocytosis.[30] Because EB1 accumulates at the plus end of growing microtubules and microtubule polymerization and depolymerization inhibition alter EB1 localization,[31] these reports presented the possibility that microtubule dynamics are important in endocytosis. It was also recently reported that paclitaxel at low concentration suppressed EGFR transport without affecting microtubule network.[32] Low concentrations of paclitaxel inhibits microtubule dynamics.[33] For these reasons, microtubule dynamics themselves are thought to be important in endocytosis. I thus analyzed the effect of microtubule dynamics on endocytosis using AG1, as a "Bioprobe", as described in the next section.

3. Materials and Methods

3.1. Fluorescent probes, antibodies and radio isotope compounds

Fluorescent probes, antibodies and radio isotope compounds are described in the Supplement 1.

3.2. Mediums

Mediums are described in Supplements 2-3.

3.3. Buffers

Buffers are described in Supplements 4-6.

3.4. Small molecules

AG1 and the derivatives were synthesized as described previously.[34] Colchicine was purchased from Sigma (Cat# C-9754, St. Louis, MO). Paclitaxel (Cat# 163-18614) and vinblastine (Cat# 221-00751) were purchased from Wako (Osaka, Japan). Human recombinant EGF (Cat# 236-EG-200) was purchased from Research & Diagnostics Systems Inc (Minneapolis, MN). All chemicals were dissolved in dimethyl sulfoxide

(DMSO, Cat# 13407-45, Nacalai Tesque). EGF was dissolved in 10 mM acetic acid.

3.5. Drug binding assay using [³H]-labeled compounds

αβ-Tubulin heterodimer was purified from porcine brain using high-molality PIPES (piperazine-1, 4-bis(2-ethanesulfonic acid)) buffer, as described,[35] and competition assay was performed as described.[36] αβ-Tubulin (0.5 mg/mL, approx. 5 µM) was mixed with non-radio labeled compounds (DMSO control, AG1, colchicine or vinblastine, final conc. 100 µM) in RB buffer (Supplement 4), and incubated at room temperature (RT) for 5 min. [³H]-Labeled colchicine or vinblastine was then added (final conc. 50 nM), and the mixture was incubated at RT for 5 min (reaction volume, 50 µL). The protein fraction was separated by centrifugal gel filtration using Centri-Spin 20 (Cat# CS-201, Princeton Separations, Freehold, NJ). The [³H]-activity of the protein fractions was detected using a liquid scintillation counter (LS 6500, Beckman Coulter, Brea, CA).

3.6. *In vitro* microtubule polymerization assay.

A microtubule polymerization assay was performed as described.[37,38] First, 1 mg/mL porcine brain tubulin was mixed with glutamate (final conc. 1 M) and GTP (final conc. 1 mM) in RB buffer (Supplement 4) on ice. Compounds (final conc. 10 µM) were

added and incubated for 10 min on ice. Samples were transferred into cuvettes, and the absorbance at 350 nm was monitored for 40 min at 2-min intervals at 37°C using a thermostatic spectrophotometer (Beckman Coulter).

3.7. Transfection and measurement of the microtubule dynamics in cells

PtK2 cells were cultured in Dulbecco's modified Eagle's medium (DMEM) supplemented with 10% (v/v) fetal calf serum (FCS) in a humidified atmosphere containing 5% CO_2. The transfection of EGFP-α-tubulin expression vector was performed using HuGene HD (Roche) according to manufacturer's protocol for 36 hrs. After the transfection, the microtubule dynamics were monitored under a microscope controlled by DeltaVision SoftWorx (Applied Precision, Issaquah, WA) using a ×60/1.40 oil immersion objective at 37°C. The cells were treated with 1 μM AG1, and three sections at 0.4 μm intervals were collected every 4 seconds for 5 min as described.[39]

The positions of the microtubule ends were traced using ImageJ software and then graphed as life history plots.[40] The speeds of growth and shortening were calculated from the slopes of the plots using linear regression. I defined the microtubule growth or shortening as the changes in the position of the microtubule end were greater than 0.5 μm between two successive time points. I defined catastrophe as the transition from either

23

growth or pause to shortening, and the rescue as the transition from shortening to either growth or pause. I calculated the catastrophe frequency by dividing the number of catastrophe by the time of growth and pause, and the rescue frequency by dividing the number of rescues by the time spent shortening.

3.8. EGF-stimulated EGFR transport analysis

HeLa cells (3 x 10^4 cells/mL/well in a 12 well plate (cat# 3815-012, Asahi Glass Co. [AGC], Tokyo) was cultured in DMEM without FCS in a humidified atmosphere containing 5% CO_2 for 7 hrs. After treatment with each compounds (DMSO control [1% v/v], 3 μM AG1, 10 nM paclitaxel, or 3 nM vinblastine) for 1 h, the serum-starved HeLa cells were treated with EGF (100 ng/mL). After 20 min, the cells were washed with phosphate-buffered saline (PBS) and immediately fixed with cold methanol (-20°C). After blocking with PBS (Supplement 5) containing 0.5% bovine serum albumin (BSA; cat# A8022, Sigma, St. Louis, MO), cells were incubated with anti-EGFR and α-tubulin antibodies. After staining with Alexa[488]-conjugated anti-mouse IgG and Alexa[568]-conjugated anti-rabbit IgG, the cells were washed four times with PBS and mounted with PBS containing 0.1 μg/mL DAPI. Microtubule networks and EGFR localizations were observed under a fluorescent microscope (Leica LAS AF 6000, Leica

Microsystems, Wetzlar, Germany).

3.9. EGF-incorporation analysis using a flow cytometer

Serum-starved HeLa cells (3×10^4 cells/mL in a 12 well plate) were treated with or without 3 μM AG1 for 1 h. The cells were then incubated with 1 μg /mL of Alexa[488]-conjugated EGF for 15 min and harvested. After the cells were washed with PBS and fixed with 3.7% formaldehyde in PBS, the EGF signal intensity was monitored by an acorstic flow cytometer (Attune, Life Technologies).

3.10. Analysis of the EGF-stimulated EGFR signal by immunoblotting

HeLa cells (1×10^5 cells/mL in a 12 well plate) were cultured in DMEM without FCS in a humidified atmosphere containing 5% CO_2 for 7 h. After treatment with or without 3 μM AG1 for 1 h, serum-starved HeLa cells were treated with EGF (10 ng/mL). At several time points (0, 5, 30, 60 and 120 min), the cells were washed with cold PBS twice and lyzed using 1 x Sodium Lauryl Sulfate (SDS) sample buffer (Supplement 6). Proteins were immunoblotted with primary antibodies (anti-EGFR, anti-p-EGFR, anti-ERK, anti-p-ERK and anti-actin antibodies) and then secondly antibodies (HRP-conjugated anti mouse and rabbit IgG). The antibodies and the dilution ratio are

described in Supplement 1.

3.11. Analysis of EGF-effect on cell viability

A431 cells (3 x 10^3 cells/100 µL/well in a 96 well plate (cat# 3860-096, AGC)) were cultured in DMEM with 0.5% FCS in a humidified atmosphere containing 5% CO_2. After treatment with or without 2 µM AG1 for 1 h, the cells were treated with various concentrations of EGF (0, 30 and 100 ng/mL). After incubation for 24 hrs, the viability of the cells was measured using the cell-counting kit-8 (Dojindo, Kumamoto, Japan).

4. Results

4.1. Effects of AG1 on the binding of colchicine and vinblastine

To estimate the AG1 binding site on the tubulin heterodimer, I performed a competition assay using the [^{3}H]-labeled tubulin inhibitors, colchicine and vinblastine, which bind to the colchicine-binding site and *vinca* alkaloid-binding site, respectively (Fig. 6). The binding of [^{3}H]-colchicine on tubulin was inhibited by cold colchicine, but enhanced by cold vinblastine. In contrast, the binding of [^{3}H]-vinblastine on tubulin was inhibited by cold vinblastine, but enhanced by cold colchicine. AG1 inhibited the binding of [^{3}H]-colchicine on the tubulin heterodimer but not of [^{3}H]-vinblastine. Interestingly, unlike colchicine, AG1 did not enhanced the binding of [^{3}H]-vinblastine. These results strongly indicate that AG1 binds to same site or a site near the colchicine-binding site, but its effects on the structure of the tubulin heterodimer were different from those of colchicine.

4.2. Effects of AG1 on microtubule dynamics

In the structure-activity relationships (SAR) study of synthetic AG1 derivatives, Hayakawa *et al*. reported that the structure of the B-ring is important for the toxicity

against HeLa cells, but some modification of hydroxyl moiety at position 7 of A ring increased the toxicity against HeLa cells (Fig. 1).[34] For example, B-ring-modified 3'4'-dimethoxyl AG1 showed very markedly decreased cytotoxicity against HeLa cells, but O^7-propargyl AG1 was the most potent inhibitor of cell-cycle progression. However, there is no information about the effects of these compounds on microtubule polymerization. I therefore investigated the effects of 3'4'-dimethoxyl and O^7-propargyl AG1 on tubulin polymerization *in vitro* (Fig. 7). O^7-propargyl AG1 potently attenuated tubulin polymerization but 3'4'-dimethoxy AG1 did not. These results suggest that hydroxyl moiety at position 7 is possible to be modified to create more potent AG1 derivatives.

Previous studies showed that AG1 delays microtubule polymerization *in vitro* and decreases the EB1-signal in cells, suggesting that AG1 may inhibits microtubule dynamics in cells. I thus investigated the effects of AG1 on microtubule dynamics. EGFP-α-tubulin-expressing Ptk2 cells were treated with DMSO (control) or 1 μM AG1 and the microtubule dynamics were measured (Fig. 8 and Table 2). AG1 increased the pause-state population (from 27.3 to 71.7 %) by decreasing the velocities of growth (from 11.2 to 5.3 μm min^{-1}) and shortening (from 13.0 to 6.2 μm min^{-1}) and the catastrophe frequency (from 0.055 to 0.024 s^{-1}). These data clearly showed that AG1 suppressed the

microtubule dynamics in the cells.

4.3. Effects of AG1 on endocytosis

It is widely thought that microtubules are important for endocytosis as the 'highway' or 'railway' of endosomes. One of the most well-studied endocytosis system is EGFR transduction. EGF stimulates the dimerization of EGFR at the cell-surface, resulting in auto phosphorylation, the activation of signal transduction pathways including ERK kinase and PI3K pathways, and internalization into early endosome and transportation. The transient activation of signal transduction and subsequent down-regulations occur during endosome maturation (acidification).[41] However, whether the function of microtubule dynamics is involved in endocytosis or not remains to be revealed. It was reported that EB1 is important for phagocytosis[30] and that paclitaxel suppress EGFR transport without affecting on microtubule network at low concentration.[32] For these reasons, microtubule dynamics might be important in endocytosis, I therefore tested the effect of AG1 and other microtubule inhibitors on endocytosis.

4.3.1 Effects of AG1 on EGF-stimulated EGFR transport

Serum starved HeLa cells were pretreated with or without compounds for 1 h, and

added with recombinant EGF. After a 20-min incubation, the cells were fixed and stained

using anti-EGFR and α-tubulin antibodies. In control cells, EGFR was transported to the

vicinity of the nucleus. In the AG1-treated cells, EGFR was distributed in the cytoplasm

without apparent disturbance of the microtubule network (Fig. 9). In this condition, the

incorporation of EGFR was not inhibited by AG1 (Fig. 10). These data suggested that AG1

inhibits the transport of endosomes through the inhibition of microtubule dynamics. The

same results were observed in the cells treated with paclitaxel or vinblastine at the

concentrations showing no apparent effects on the microtubule network (Fig. 11),

suggesting that the inhibition of endosome transport is not due to the inhibition of another

target molecules by AG1, and microtubule dynamics are important in endosome transport.

4.3.2. The effects of AG1 on the signal activated by EGF

To analyze the effect of AG1 on the down-regulation of EGFR signaling,[42] I

observed the phosphorylations of EGFR and ERK, which is the downstream of EGFR (Fig.

12). In control cells, EGFR and ERK were phosphorylated immediately (within 5 min) and

dephosphorylated completely within 2 h after treatment. In contrast, AG1 prolonged the

EGFR and ERK phosphorylations until 2 h after treatment. This results suggest that AG1

suppresses endosome maturation by an inhibition of microtubule dynamics.

4.3.3. The effects of EGF and AG1 on EGFR-over-expression cell line A431

There are several reports that prolonged EGFR signaling induces cell death in EGFR-overexpressing cells.[43,44] As described in the previous section, AG1 prolonged the phosphorylations of EGFR and ERK kinases, I therefore expected that AG1 also induces EGF-dependent cell death. To test this hypothesis, I used serum-starved A431 cells, which overexpress EGFR. A431 cells were pretreated with AG1 for 1 h, followed by treatment with various concentrations of EGF. The growth of AG1-treated cells was inhibited by EGF in a dose-dependent manner (Fig. 13). This result suggesting that AG1 induces cell death by not only the mitotic arrest but also the inhibition of endosome maturation.

5. Conclusions and discussion

Here I observed that AG1 binds to the colchicine site on the tubulin heterodimer and inhibits microtubule dynamics in mammalian cells. My finding also indicated that AG1 suppresses endosome maturation and induces EGF-dependent cell death in EGFR-overexpressing cells by inhibiting microtubule dynamics.

I estimated the binding site of AG1 by conducting a competition assay using [3H]-vinblastine and [3H]-colchicine, well-known microtubule polymerization inhibitors. The binding of [3H]-colchicine on tubulin was inhibited by cold colchicine, but enhanced by cold vinblastine, whereas the binding of [3H]-vinblastine on tubulin was inhibited by cold vinblastine, but enhanced by cold colchicine. It is known that colchicine and vinblastine, induce similar curved conformations of tubulin,[28,29] and the binding of colchicine opens the binding site of vinblastine. Like colchicine, AG1 inhibited the binding of [3H]-colchicine on the tubulin heterodimer but not the binding of [3H]-vinblastine. Interestingly, AG1 did not enhance the binding of [3H]-vinblastine like colchicine did, suggesting that AG1 binds at same site of colchicine or a nearby site, but its effects on the structure of the tubulin heterodimer were different from those of colchicine or vinblastine. These difference in conformational changes between AG1 and colchicine might underlie their different effects on tubulin de-polymerization.

The effects of AG1 on tubulin polymerization *in vitro* and EB1 signals in cells suggested

that AG1 inhibits microtubule dynamics by attenuating microtubule polymerization. However, no information is available regarding the effect of AG1 on microtubule shortening. To reveal the effects of AG1 on microtubule in detail, it is important to obtain direct evidence that AG1 inhibits microtubule dynamics in cells. By observing microtubule dynamics in PtK2 cells, I found that AG1 suppresses microtubule dynamics. AG1 increased the pause-state population by decreasing the velocities of growth and shortening, and the catastrophe frequency. Furthermore, the mode of action of AG1 on microtubule dynamics is different from another microtubule dynamics inhibitor, eriburin, but similar with noscapine. Noscapine increased the pause-state population by decreasing the velocities of growth and shortening and the catastrophe frequency like AG1.[40] However, eriburin inhibits microtubule elongation but not shortening.[9,10] Therefore, it is also important to elucidate the differences between AG1 and eriburin for an understanding how microtubule dynamics inhibitors affect microtubule dynamics.

I also used AG1 as a tool to investigate the role of microtubule dynamics in endocytosis, and the results suggested that AG1 inhibits endosome maturation and induces cell death in an EGF-dose dependent manner. These finding imply that microtubule dynamics, seamless growth and shortening of microtubule ends, is important for proper endosome transport and maturation and that microtubule dynamics inhibitors induces cell death by two pathways, the inhibition of mitotic spindle and the inhibition of endosome maturation, by inhibiting microtubule dynamics. These

results also demonstrated that AG1 will be a useful tool for investigations of the function of microtubule dynamics in cells.

Although the finding described in this chapter indicate that AG1 binds to the colchicine binding site and inhibits microtubule dynamics, the details of the binding mode, further information about amino acid residues that are important for AG1 binding on the tubulin heterodimer, and the mechanism of microtubule dynamics inhibition are still unclear. It is important to elucidate the differences in binding mode between AG1 and colchicine for a greater understanding how AG1 inhibits microtubule dynamics but not polymerization.

To understand differences between AG1 and colchicine or eriburin, the one way is analysis of their binding mode by genetic approach using model organisms such as *S. cerevisiae*, and the other way is analysis of their effect on the conformation change of tubulin heterodimer. By these analysis, I can reveal the properties of microtubule dynamics regulation in detail.

6. Figures and tables
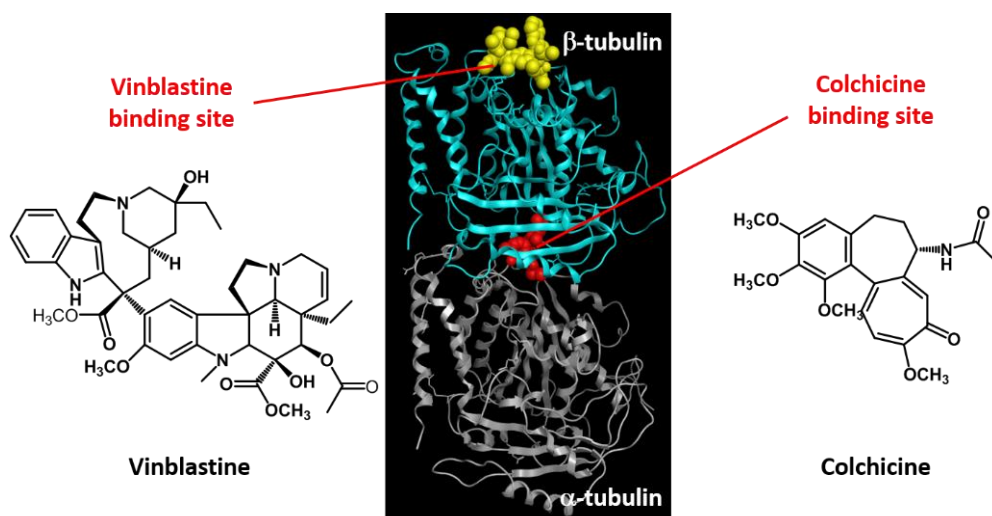
Fig. 5. The binding sites of colchicine and vinblastine on the tubulin heterodimer.[28,29]

The binding sites of colchicine and vinblastine on β-tubulin are shown. Vinblastine (yellow molecule) binds the interphase of two heterodimers. Colchicine (red molecule) binds the interphase between α- and β-tubulin in the tubulin heterodimer.
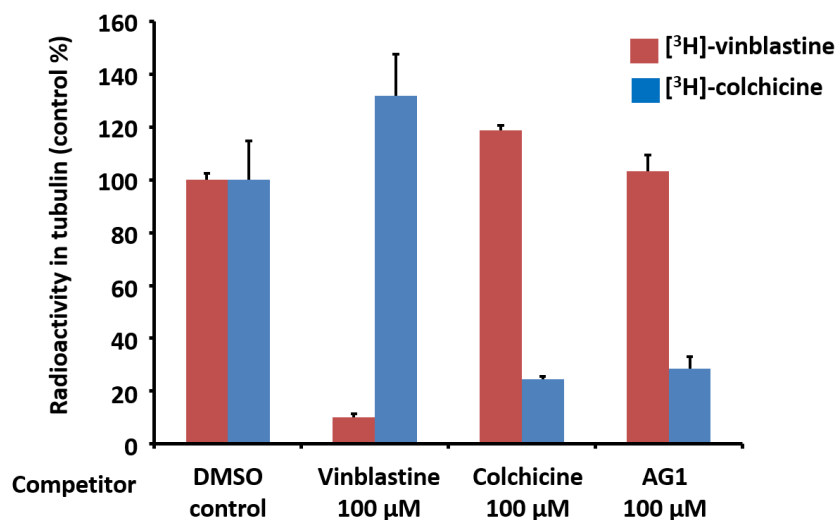
Fig. 6. Competition analysis using [³H]-compounds.

Porcine brain α/β-tubulin (0.5 mg/mL, approx. 5 µM) was mixed with 100 µM of non-radio labeled compounds (DMSO control, AG1, colchicine or vinblastine), and incubated at RT for 5 min. Then 50 nM of [³H]-labeled colchicine or vinblastine was added and incubated at RT for 5 min. The protein fraction was separated by centrifugal gel filtration using a Centri-Spin 20, and the [³H]-activity of the tubulin fractions was detected.
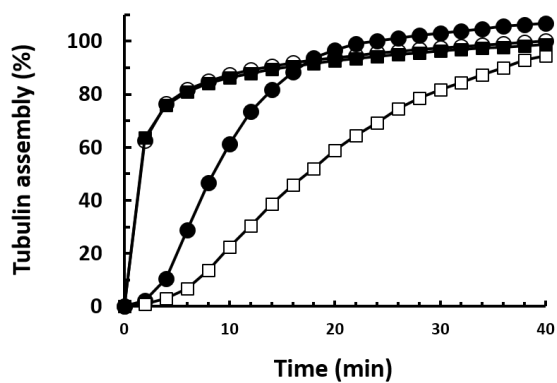
Fig. 7. The effect of AG1 derivatives on tubulin polymerization.

First, 1 mg/mL tubulin purified from porcine brain was mixed with each compounds. Tubulin polymerization was determined by measuring the absorbance at 350 nm. Open and closed circles are DMSO control and 10 μM of AG1, respectively. Close and opend squares are 10 μM of 3'4'-dimethoxy AG1 and 10 μM of O^7-propargyl AG1, respectively.

DMSO
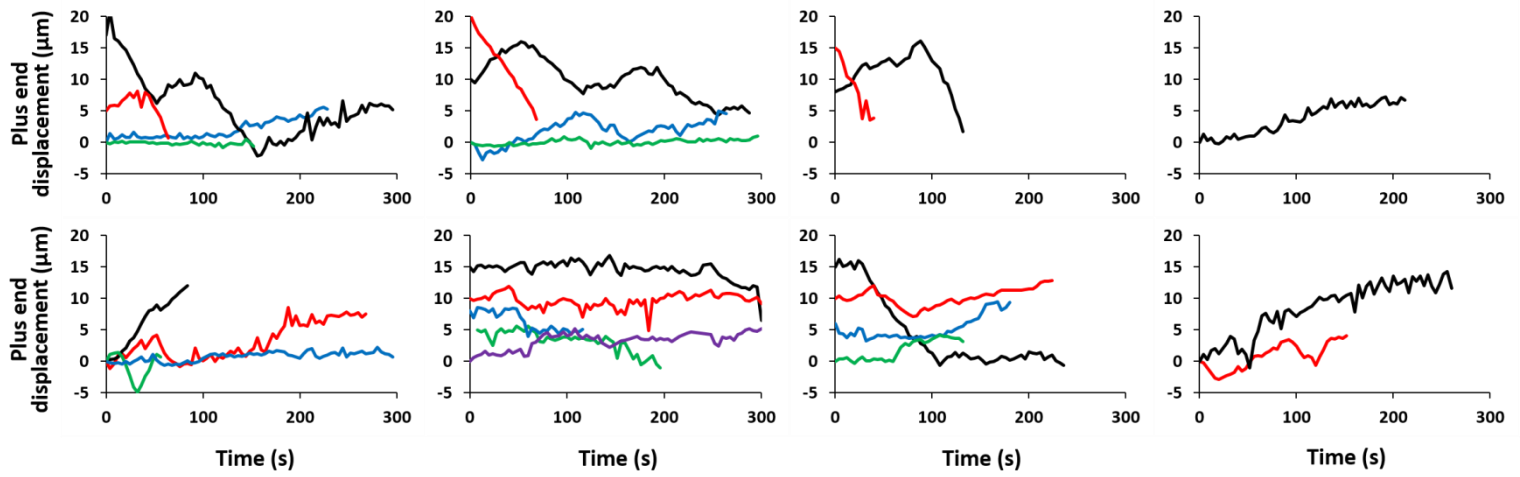
2 µM AG1
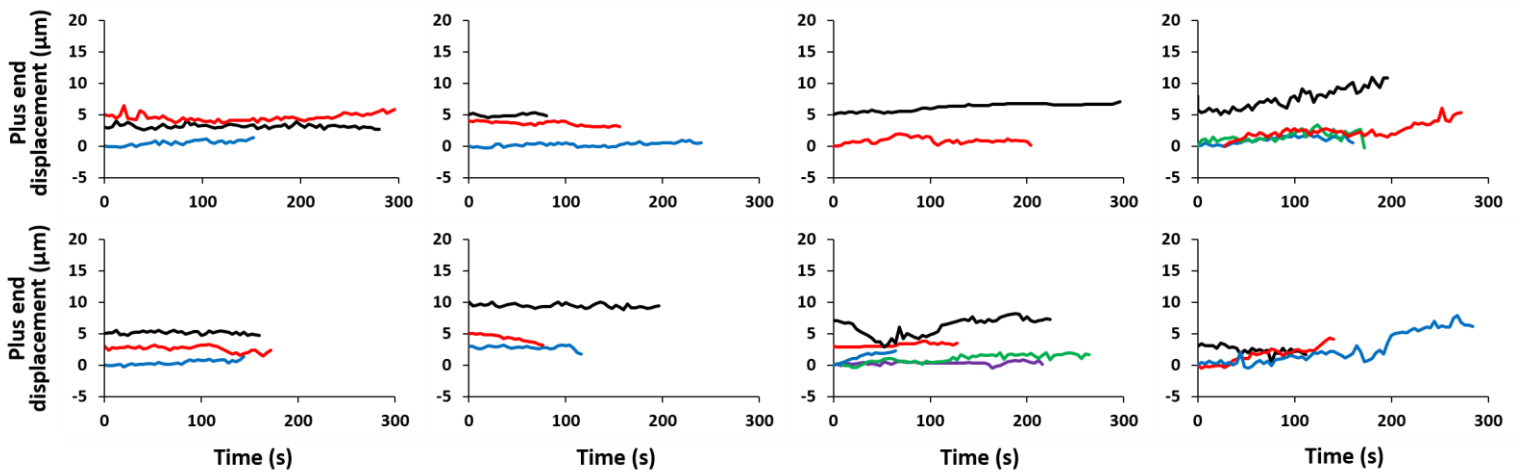
Fig. 8. The effect of AG1 on the microtubule dynamics in cells.

EGFP-α-tubulin-expressing Ptk2 cells were treated with 1 µM AG1, and three sections at 0.4 µm intervals were collected every 4 s as described in the Materials and Methods section. The positions of the microtubule ends were followed using ImageJ software and graphed as life history plots. Total 26 microtubules in DMSO or AG1 treated cells were analyzed.
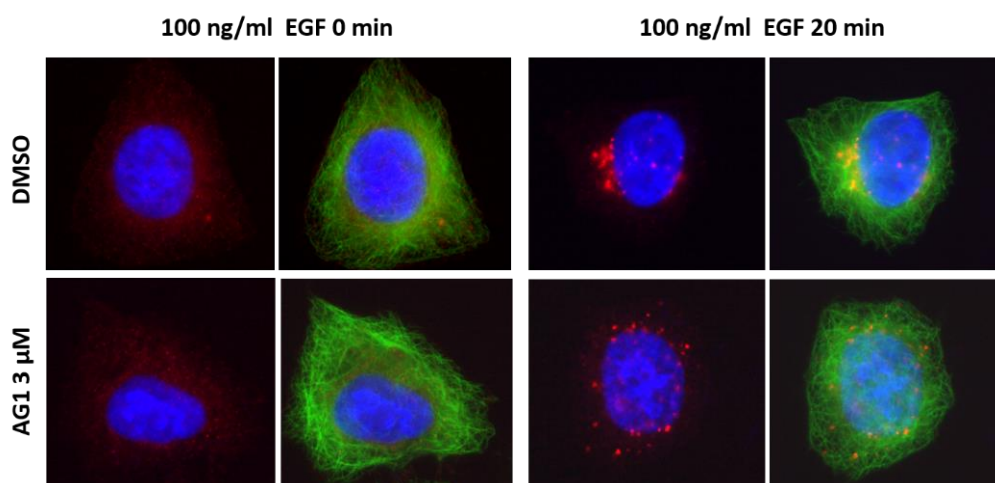
Fig. 9. The effect of AG1 on EGF-stimulated EGFR transport.

Serum-starved HeLa cells were treated with each compound (DMSO control [1% v/v] or 3 μM AG1) for 1 h, then treated with EGF (100 ng/mL). After 20 min, cells were fixed and stained as described in the Materials and Methods section. Microtubule networks and EGFR localizations were observed by fluorescent microscopy. Green, red and blue represent α-tubulin, EGFR and DNA, respectively.
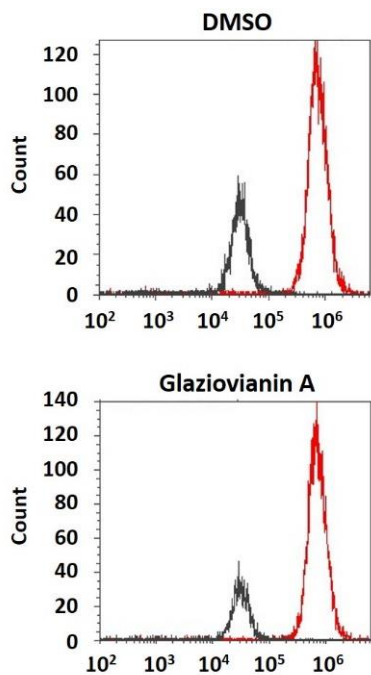
Fig. 10. The effect of AG1 on EGF incorporation.

Serum-starved HeLa cells were treated with or without 3 μM AG1 for 1 h, then incubated with 1 μg/mL of Alexa[488]-conjugated EGF for 15 min and harvested. After washing and fixation, the EGF signal intensity was monitored by an acoustic flow cytometer. Black and red peaks represent the signals of the cells before and after Alexa[488]-conjugated EGF treatment, respectively.
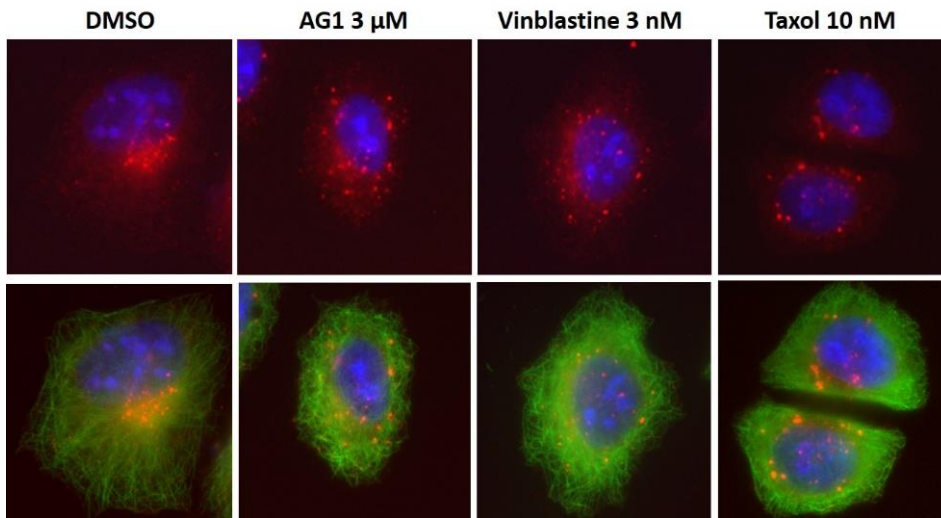
Fig. 11. The effect of microtubule inhibitors on EGF-stimulated EGFR transport.

Serum-starved HeLa cells were treated with each compound (DMSO control [1% v/v], 10 nM paclitaxel, or 3 nM vinblastine) for 1 h, then treated with EGF (100 ng/mL). After 20 min, the cells were fixed and stained as described in the Materials and Methods section. Microtubule networks and EGFR localizations were observed under a fluorescent microscope.
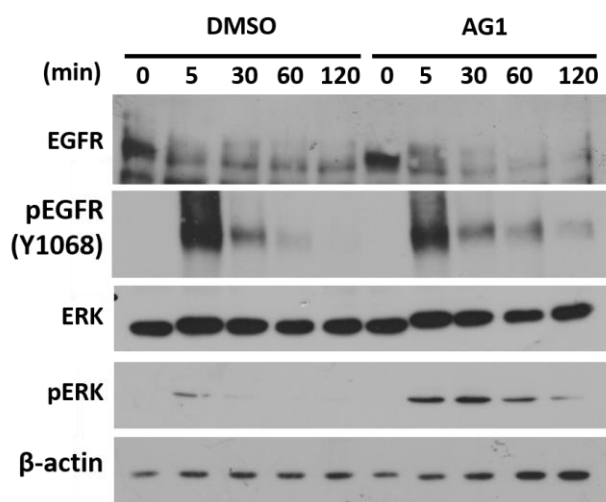
Fig. 12. The effect of AG1 on the signal activated by EGF.

After treatment with or without 3 μM AG1 for 1 h, serum-starved HeLa cells were treated with EGF (10 ng/mL). At each time point (0, 5, 30, 60 and 120 min), proteins were detected by immunoblotting using anti-EGFR, anti-p-EGFR, anti-ERK, anti-p-ERK and anti-actin antibodies.
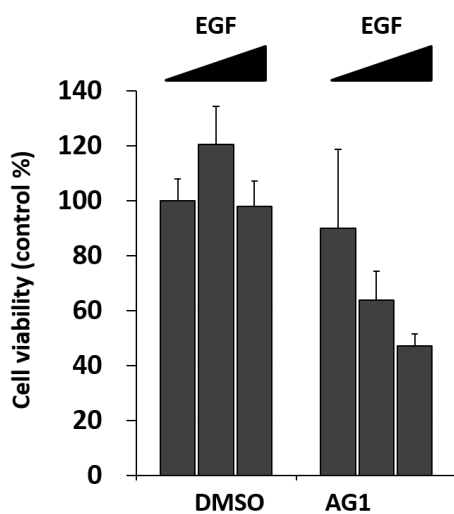
Fig. 13. The effects of EGF and AG1 on the EGFR-over expressing cell line A431.

After treatment with or without 2 μM AG1 for 1 h, A431 cells (cultured with 0.5% FCS) were treated with various concentrations of EGF (0, 30, and 100 ng/mL). After incubation for 24 h, the viability of the cells was measured using a cell-counting kit-8 (WST-8).

	growth (μm min^{-1})	shortening (μm min^{-1})	catastrophe frequency (s^{-1})	rescue frequency (s^{-1})	time in		
					growth %	pause %	shortening %
DMSO	11.2 ± 1.4	13.0 ± 1.1	0.055 ± 0.007	0.113 ± 0.011	37.3	27.3	35.5
glaziovian A	5.3 ± 0.7*	6.2 ± 0.7*	0.024 ± 0.005*	0.119 ± 0.015	16.0	71.7	12.3

Table 2. Parameters of microtubule dynamics

The rates of microtubule growing and shortening were calculated from the slopes of life history plots of 26 microtubules from five control cells and 26 microtubules from eight AG1-treated cells (Fig. 8) as described in the Materials and Methods section. Values are means ± SE. *, $P \leq 0.01$.

CHAPTER 3. Construction of a multidrug hyper-sensitive yeast for analysis of AG1

1. Summary

I constructed a yeast strain with multidrug hyper-sensitivity and the sufficient efficiency for genetic analysis, 12geneΔ0HSR-iERG6, to analyze the molecular basis of the inhibitory mechanism of AG1 on tubulin. First, 12geneΔ0 was created by the disruption of 12 genes involved in the drug efflux system (eight ABC transporters on the plasma membrane and their four transcriptional factors) in BY4741, the parental yeast strain. The constructed strain retained mating and transformation efficiencies comparable to those of BY4741, but it showed decreased sporulation efficiency, one of the key properties needed for genetic analyses. I therefore introduced the *RME1*-(ins-308A) mutation to increase the sporulation efficiency, and the created strain was named 12geneΔ0HSR (12geneΔ0 High Sporulation with *RME1*).

The 12geneΔ0HSR strain showed multidrug sensitivity and a level of sporulation efficiency comparable to that of BY4741. However, the strain did not show AG1 sensitivity. Because the spectrum of drug resistance dependent on the drug efflux system and the spectrum of permeability barrier system are different, I next introduced the conditional expression promoter in *ERG6* gene to disrupt the drug permeability barrier system in 12geneΔ0HSR. The newly

constructed strain, 12geneΔ0HSR-iERG6, showed improved sensitivities to several compounds including O^7-propargyl AG1 under the glucose condition, and it exhibited sufficient transformation and sporulation efficiencies under the galactose condition. Because of its high sensitivities to several compounds, 12geneΔ0HSR-iERG6 strain will be a useful tool not only for investigation of the inhibitory mechanism of AG1 but also for chemical biology studies.

2. Introduction

As described in Chapter 2, AG1 binds to the colchicine binding site on the tubulin heterodimer and inhibits microtubule dynamics, but the details of the binding mode and the mechanism of the suppression of microtubule dynamics are still unclear. Mammalian cells have around 8 α- and 8 β-tubulin isoforms, and the several post-translational modifications of microtubules such as acetylation, phosphorylation, polyglutamylation and polyglycylation are known.[18] This tubulin heterogeneity makes the further analysis difficult, and a simpler system is desired to reveal the detailed inhibitory mechanism of AG1 on microtubules.

S. cerevisiae has only two α-tubulin isoforms (Tub1p and Tub3p) and one β-tubulin isoform (Tub2p), and *TUB3* gene can be deleted because *TUB3* null mutant is viable.[20] Therefore *S. cerevisiae can* express a single allele of the α/β-tubulin isoform from *TUB1* and *TUB2* genes, and genetic modification of these genes are useful in analyses of the mode of action of microtubule inhibitors (including AG1) *in vitro* and *in vivo.*[21] However, there is a major obstacle in mode-of-action analyses using *S. cerevisiae*. *S. cerevisiae* is resistant to most of the compounds to which mammalian cells are sensitive (Table 1). Because this multidrug resistance makes analyses difficult, new strains showing high sensitivities to AG1 are required for the analysis of the mode of action of AG1.

There are two factors conferring multidrug resistance in *S. cerevisiae*, one is the drug efflux

system, and the other is the permeability barrier. The drug efflux system is composed of ABC transporters that export xenotoxic compounds to outside the cells or inside the vacuole.[24–26] The major factor for the permeability barrier is ergosterol in the yeast plasma membrane. To make yeast sensitive to several compounds, the disruption of ergosterol synthetic genes (*ERG* genes, e.g., *ERG6* and *ERG3*) is thus frequently applied. However, *ERG6* disruption decreases the transformation, mating and sporulation efficiencies, which are needed for genetic analyses. I therefore speculated that it is possible to create a strain that is highly sensitive to multiple drugs, not only by the disruption of ABC transporter that involved in only drug efflux system, but also by the introducing the an *ERG6*-inducible system.

S. cerevisiae has at least 16 ABC transporters, of which Pdr5p, Snq2p and Yor1p confer multidrug resistance by exporting bioactive small molecules to outside of cells. Four transcriptional factors, Pdr1p, Pdr3p, Pdr8p and Yrr1p, up-regulate the transcription of most of these ABC transporters. Here I first focused on the ABC transporters that exist only on the plasma membrane (including Pdr5p, Snq2p and Yor1p) and their transcription factors, because some ABC proteins are essential for cell viability, ion homeostasis, organelle development and so on. The constructed strain lacking eight ABC transporters and four transcription factors showed sensitivity to several compounds, but was not sensitive to AG1 and AG1 derivatives. I therefore introduced the *ERG6*-inducible expression system, and succeeded in constructing a strain showing the sensitivity

to AG1 derivative, O^7-propargyl AG1.

3. Materials and Methods

3.1. Yeast strain

In this study, BY4741[45] (*MATa his3Δ1 leu2Δ0 met15Δ0 ura3Δ0*) and BY4742[45]

(*MATα his3Δ1 leu2Δ0 met15Δ0 ura3Δ0*) were used as parental strains.

3.2. Primers and plasmids

Primers and plasmids are described in Tables 3 and 4, respectively.

3.3. Mediums

Mediums are described in Supplements 7 - 16. The final concentrations of 1.5%

(w/v) agar was added to medium described in Supplements 7 – 16 to make solid medium.

3.4. Buffers

Buffers used are described in Supplements 17 - 19.

3.5. Small molecules

Digitonin (Cat# D141), fluphenagine (Cat# F4765), hygromycin B (Cat# H-7772),

nocodazole (Cat# M1404) and 4-nitroquinoline 1-oxide (Cat# N8141) were purchased

from Sigma. Anisomycin (Cat# 017-16861), cycloheximide (Cat# 038-11131), diamide

(Cat# D3648), G418 (Cat# 070-05183), latrunculin A (Cat# L5163), lovastatin (Cat#

PHR1285), manoalide (Cat# 36172), menadione(Cat# M5625), rapamycin (Cat# 37094),

staurosporine(Cat# 37095), thiabendazole(Cat# T8904) and tunicamycin (Cat# T7765)

were purchased from Wako. Rhodamine 6G (Cat# 7076L) was purchased from Polyscience

(Warrington, PA). Fluconazole (Cat# F4682) and nystatin (Cat# N926000) were purchased

from LKT Laboratories (St. Paul, MN). G418 was dissolved in sterile water. Fluconazole

was dissolved in 100% ethanol. Other compounds were dissolved in DMSO (Nacalai

Tesque).

3.6. Construction of the *KanMX6-Gal1p* cassette plasmid, pTC031

To introduce the *GAL1* promoter in the *ERG6* upstream, I constructed the

KanMX6-Gal1p cassette plasmid, pTC031. *Sac*I-*GAL1* promoter-*Eco*RI DNA fragment

was amplified by PCR (Tables 5 and 6). The amplified fragment was digested by

restriction enzymes (*Sac*I/*Eco*RI) and ligated to the *Sac*I/*Eco*RI site of pYM-N1 plasmid

using a ligation high kit (Toyobo, Osaka, Japan). The ligated plasmid was transformed into

E. coli DH5α, and the sequence was confirmed using a genetic analyzer (ABI3130,

Applied Biosystems, Foster, CA).

3.7. Amplification of DNA fragments for integration

3.7.1. Cassette PCR

Cassette PCR was performed using S1- /S2- primers (template = pFA6a-*CgURA3*

or -*KanMX6*) or S1-/S4- primers (template = pTC031). PCR mixture and PCR program are

described in Tables 7 and 8, respectively.

3.7.2. DNA fragments to pop-out *CgURA3* marker

DNA fragments to pop-out *CgURA3* marker were created by a three-step of PCR

protocol (1st, annealing and 2nd). PCR was performed using the mixture and program

described in Tables 9 - 14.

3.8. Transformation of DNA fragments by the lithium acetate method

Each strains was grown in 50 mL of liquid medium at 30°C and 170 rpm in the

shaker. Cells in logarithmic growth phase (cell density OD_{600} = 0.3 - 0.4) were collected by

centrifugation at 5,000 rpm for 3 min. After being washed with 50 mL of MilliQ, the cells

were washed with 10 mL of LiSorb buffer (Supplement 17). The cells were then

re-suspended in 300 μL of LiSorb buffer. Fifty μL of yeast in Lisorb buffer was added to 300 μL LiPEG buffer (Supplement 18) containing 5 μL of PCR product or plasmid and 5 μL of carrier DNA, and incubated at RT for 20 min. After the addition of 35 μL of DMSO to the yeast cell solution, the cells were incubated at 42ºC for 15 min. After they cooled down on ice, the cells were collected by centrifugation at 5,000 rpm for 3 min. The cells were re-suspended with 100 μL of MilliQ, and then plated on selection plates. After incubation at 30ºC for 2 - 3 days, positive clones were confirmed by colony direct PCR.

3.9. Confirmation of genetic modification by colony direct PCR and sequencing analysis

Transformants were suspended in Zymolyase buffer (Supplement 19), and incubated at 37ºC for 30 min. Zymolyase-treated samples were used for the colony direct PCR as a template. The PCR mixture and program are described in Tables 15 and 16, respectively. In addition, in *RME1* mutants, the mutation (*ins-308A*) was confirmed by a sequencing analysis using the ABI3130 system.

3.10. Mating type switch

A mating type switch from *MATa* to *MATα* was performed by the expression of HO endonuclease as described[46]. The HO endonuclease transient expression plasmid was transformed, and the transformants were incubated in YP-Raf/Gal medium. After a 4 h incubation, induction was stopped by the addition of glucose. The cells were spread on a

YPD plate. After incubation for 3 days, the mating type was tested by mating with a tester strain.

3.11. Transformation efficiency

One μg of pRS315 plasmid (containing *LEU2* marker) was transformed into each strains in the logarithmic growth phase (grown in media described in Supplement 7 or 13, OD_{600} = 0.4, 20 mL). After selection on a SC-LEU plate (Supplement 9), the numbers of colonies were counted, and colony forming units (cfu/μg) were calculated as the transformation efficiency.

3.12. Mating efficiency

Each strains (*MATa* strain harboring pRS315 [the medium is in Supplement 9] and *MATα* strains harboring pRS313 [the media is Supplement 10]) in logarithmic growth phase (OD_{600} = 0.4, 500 μL) were mixed and concentrated on a nitrocellulose membrane. After incubation at 30ºC for 6 h on a YPD plate (Supplement 7), the cells were suspended in MilliQ and plated on the SC-LEU (Supplement 9) and SC-LEU/-HIS (Supplement 11) plates. After incubation at 30ºC for 2 - 3 days, the mating efficiencies were calculated by dividing the number of colonies on the SC-LEU/-HIS plate by that on the SC-LEU plate.

3.13. Sporulation efficiency

Each strains in the logarithmic growth phase grown in the pre-sporulation medium (described in Supplement 14 or 15) was plated on a sporulation plate (Supplement 16) and incubated at RT for 1 wk. Cells showing sporulation were counted under a microscope, and sporulation efficiencies were calculated.

3.14. Drug sensitivity test by WST-8 assay

The strains were grown in YPD liquid medium (Supplement 7) at 30ºC and 170 rpm in the shaker. Cells in the logarithmic growth phase (OD_{600} = 0.1) were treated with each compounds (1% [v/v] addition). After incubation at 30ºC for 4 or 6 h, 10 μL of WST-8 (Dojindo) was added. After incubation at 30 ºC for 1 - 3 h, absorbance at 450 nm was determined using a plate reader (iMark, Bio-Rad, Hercules, CA). Inhibition rates (% of control) were calculated from the absorbance at 450 nm.

3.15. Drug sensitivity test by halo assay

The strains were grown in YPD liquid medium (Supplement 7) at 30ºC, 170 rpm in the shaker. Cells in the logarithmic growth phase were mixed in 0.5% agar (OD_{600} =

0.05) and plated on a YPD plate. Three or five µL of drug solutions was spotted on the

plates containing yeast, and the plates were incubated at 30ºC for 1 - 2 days. Drug

sensitivities were compared based on the sizes of growth inhibition areas.

4. Results

4.1 Construction of 12geneΔ0 by the two-step gene disruption method

Eight ABC transporter genes (*AUS1*, *PDR5*, *PDR10*, *PDR11*, *PDR12*, *PDR15*, *SNQ2*, and *YOR1*) and four genes of their transcriptional factors (*PDR1*, *PDR3*, *PDR8*, and *YRR1*) were disrupted in BY4741 background by the *delitto perfetto* methods,[47] a modified PCR-based marker less gene disruption method (Fig. 14A). After the deletion of a gene by replacement with the *CgURA3* marker, this marker was popped out by transformation of the DNA fragment which is directly ligated up- and down-stream sequence of target genes (Fig. 14B). The constructed strain was confirmed by colony direct PCR (Fig. 14C). Primer "GeneX-6" (forward primer) anneals upstream (200 - 300 bp) of *Gene X*, primer "GeneX-2" (reverse primer) anneals downstream (200 - 300 bp) of *Gene X,* primer "GeneX-5" (forward primer) anneals the open reading frame (ORF) of *Gene X,* and CgURA3-F （forward primer) anneals ORF of the *CgURA3* marker. Constructed strains are listed in Table 17.

4.2 Characterization of 12geneΔ0, and the transformation, mating and sporulation efficiencies of 12geneΔ0

To use 12geneΔ0 for chemical biology studies, it is important to show not only its multidrug sensitivity but also its transformation, mating and sporulation efficiencies. I therefore confirmed these efficiencies of 12geneΔ0 as described below.

4.2.1 The transformation efficiency of 12geneΔ0

The transformation efficiencies of several strains were compared. One μg of pRS315 was transformed and colony forming unit (cfu/μg) on the SC-LEU plate was determined as a transformation efficiency (Fig. 15A). 12geneΔ0 showed high transformation efficiency comparable to that of BY4741. In contrast, ergosterol deficient, especially that in the *erg6*-deficient cells, resulted in severely decreased transformation efficiency. These data suggest that *ERG6* but not ABC transporters contribute to transformation efficiency.

4.2.2. The mating efficiency of 12geneΔ0

I compared the mating efficiency of each strain. Each strain (*MATa* strain harboring pRS315 and *MATα* strains harboring pRS313) were mixed and concentrated on a nitrocellulose membrane and incubated at 30ºC for 6 h on a YPD plate. The cells were plated on the SC-LEU and SC-LEU/-HIS plates, and the mating efficiencies (diploid cell

number) were calculated by dividing the number of colonies on the SC-LEU/-HIS plate by that on the SC-LEU plate (Fig. 15B). 12geneΔ0 showed the same order of mating efficiency as that of BY4741. On the other hand, ergosterol deficient markedly decreased the mating efficiency. These results suggest that ergosterol-deficient cells are not suitable for genetic analyses.

4.2.3. The sporulation efficiency of 12geneΔ0

The sporulation efficiencies of each strain were compared. Diploid cells of each strain were grown on a plate of sporulation medium at RT for 1 wk. The cells were then observed under a microscope, and the percentage of cells with spores was calculated (Fig. 15C). The *erg3* disruptant showed sporulation efficiency comparable to that of wild type cells, but 12geneΔ0 and the *erg6* disruptant had decreased sporulation efficiency. These findings indicate that 12geneΔ0 and *erg6* disruptant are not suitable for genetic analyses and suggest that it is necessary to increase the sporulation property of 12geneΔ0 for chemical biology studies.

4.3. Improvement of the sporulation efficiency of 12geneΔ0 by introducing *RME1* (*ins-308A*) mutation

59

It was reported that single-nucleotide polymorphisms of three genes (a noncoding regulatory region of *RME1* [*ins-308A*], and two missense mutations in *TAO3* and *MKT1*) are involved in sporulation efficiency, and these mutations introduced in S288c, the parental strain of BY4741, increased sporulation efficiency.[48] I therefore introduced *RME1* (*ins-308A*) mutation, adenine insertion in the 308 bp upstream from the ATG of *RME1*, and *MKT1 (D30G)* mutation into 12geneΔ0 to improve its sporulation efficiency by a PCR-based gene replacement, which consisted of two steps (Fig. 16). *RME1* (*ins-308A*) mutation increased the sporulation efficiency (Table 18) in both BY4741 (from 21.9% to 48.8%) and 12geneΔ0 (from 5.0% to 28.8%). The *MKT1 (D30G)* mutation also increased the sporulation efficiency (Table 18) in both BY4741 (from 21.9% to 51.7%) and 12geneΔ0 (from 5.0% to 25.6%). However, it was reported that the *MKT1 (D30G)* mutant shows a petite colony in S288c background,[49] and thus I decided to use the *RME1* mutant for my thesis.

4.4. The drug sensitivity of 12geneΔ0HSR

For chemical biology studies, it is important that 12geneΔ0HSR has improved multidrug sensitivity, and thus I tested the sensitivities of 1-12geneΔ0 and 12geneΔ0HSR in the liquid medium. The drug sensitivities of several strains were compared in the YPD

liquid medium by WST-8 assay. Cells in the logarithmic growth phase ($OD_{600} = 0.1$) were treated with several concentrations of compounds and incubated at 30ºC for 4 h. The concentrations that inhibited the growth at 50 % (i.e., IC_{50}) were calculated from growth inhibition curves (Figure 17 and Table 19). The sensitivities against staurosporine, 4-nitroquinoline 1-oxide and latrunculin A were increased as the number of deleted genes increased (Fig. 17). Especially, latrunculin A sensitivity was drastically increased by *PDR5* disruption. In addition, gene disruption of ABC transporters in 4geneΔ, transcriptional factors deleted strain, increased sensitivity drastically. These results suggest that drug efflux system based on ABC transporters works redundantly and basal expression of ABC transporters confer multidrug resistance. 12geneΔ0HSR basically showed higher sensitivities to several compounds than BY4741, the parental strain. However, 12geneΔ0HSR did not show drastically increased sensitivities to hygromycin B and fulphenazine, whereas the *erg6* disruptant showed quite high sensitivities to these compounds (Table 19). These results suggest that ABC transporters and ergosterol confer drug resistance to different group of compounds, and that *ERG6* gene is important target for creating multidrug-sensitive strain.

4.5. The effect of AG1 derivatives on 12geneΔ0HSR

To analyze the effects of AG1 derivatives using yeast, I determined the effects of AG1 derivatives on the growth of 12geneΔ0HSR by conducting a halo assay. AG1 and the high active derivative O^7-propargyl AG1 did not show the toxicity against 12geneΔ0HSR (Fig. 18). These results suggest suggest that the sensitivity of 12geneΔ0HSR is not enough to analyze the mode of action of AG1.

4.6. The construction of 12geneΔ0HSR-iERG6, a multidrug-sensitive strain conditionally expressing *ERG6* gene under the Gal1 promoter

To improve the sensitivities to compounds to which yeast shows resistance by permeability barrier, I constructed an *ERG6* conditional expression strain (12geneΔ0HSR-iERG6) by the genome integration of a PCR fragment (*KanMX6-Gal1p*) into the 5'-UTR of *ERG6* gene of 12geneΔ0HSR. The construction of this strain was confirmed by direct PCR (Fig. 19). We also constructed *erg6* disruptant (12geneΔ0HSR *erg6Δ::KanMX6*) in 12geneΔ0HSR background as a reference. The sensitivity to latruncurin A but not to hygromycin B was increased in 12geneΔ0HSR. On the other hand, the sensitivity to hygromycin B was increased in *erg6Δ* strain even in the wild type background (Table 19).[50] I thus expected that 12geneΔ0HSR-iERG6 would be sensitive to

62

hygromycin B in the presence of glucose and show sufficient transformation, mating and

sporulation efficiency in the presence of galactose (Fig. 20).

4.7. The drug sensitivity testing of 12geneΔ0HSR-iERG6

It is important that 12geneΔ0HSR-iERG6 shows improved multidrug sensitivity.

Because *Gal1* promoter is down-regulated in the presence of glucose but up-regulated in

both the presence of galactose and the absence of glucose, the constructed strain was

expected to show drug sensitivities under the glucose condition. I thus tested the strain's

sensitivities in liquid and on solid medium by a WST-8 and a halo assays under the glucose

condition.

4.7.1. The drug sensitivity testing by WST-8 assay

The drug sensitivities of several strains were compared in YPD liquid medium

(glucose condition). Cells in the logarithmic growth phase ($OD_{600} = 0.1$) were treated with

varying concentrations of compounds and incubated at 30ºC for 6 h. The concentrations

which inhibits the growth at 50 % (IC_{50}) were calculated from the growth inhibition curves

(Table 20). 12geneΔ0HSR-iERG6 and 12geneΔ0HSR *erg6Δ::KanMX6* showed improved

multidrug hyper sensitivity to latrunculin A (efflux system-dependent resistance),

hygromycin B and fluphenazine (permeability barrier system-dependent resistance).

4.7.2. The drug sensitivity testing by halo assay

I compared the drug sensitivities of each strain on the YPD plate (glucose condition) by performing halo assay. With this method, it is possible to compare the drug sensitivity by observation of the growth inhibition areas that are drug-spotted. 12geneΔ0HSR-iERG6 showed improved drug sensitivity, comparable to that of 12geneΔ0HSR *erg6Δ::KanMX6* (Fig. 21).

4.8 The transformation, mating and sporulation efficiency of constructed strains

To use 12geneΔ0HSR-iERG6 for chemical biology studies, it is also important to determine its transformation, mating and sporulation efficiencies. Because *Gal1* promoter is up-regulated in both the presence of galactose and the absence of glucose, the constructed strain was expected to show good efficiencies under the galactose condition but not under the glucose condition. I therefore tested the strain's transformation, mating and sporulation efficiencies under the both condition.

4.8.1 The transformation efficiency of 12geneΔ0HSR-iERG6

I compared the transformation efficiencies of each strains. Under the YPD culture condition, 12geneΔ0HSR-iERG6 showed quite low transformation efficiency, comparable to that of 12geneΔ0HSR *erg6Δ::KanMX6.* In contrast, under the YP-Raf/Gal culture condition, 12geneΔ0HSR-iERG6 showed high transformation efficiency, comparable to that of 12geneΔ0HSR (Fig. 22A). These results showed that it is able to transform DNA into 12geneΔ0HSR-iERG6 under the YP-Raf/Gal culture condition.

4.8.2. The mating efficiency of 12geneΔ0HSR-iERG6

The mating efficiencies of each strains were also compared. Under the YPD culture condition, 12geneΔ0HSR-iERG6 and 12geneΔ0HSR *erg6Δ::KanMX6* showed sufficient mating efficiency comparable to that of 12geneΔ0HSR (Fig. 22B), indicating that *ERG6* disruption in 12geneΔ0HSR does not affect its mating efficiency.

4.8.3. The sporulation efficiency of 12geneΔ0HSR-iERG6

The sporulation efficiencies of each strains were evaluated. Diploid cells of each strains were grown on a plate of sporulation medium at RT for 1 wk. The cells were then observed under a microscope, and the percentage of cells with spores was calculated.

Under the glucose condition, 12geneΔ0HSR-iERG6 did not make spore, whereas made spore under the galactose condition (Fig. 22C). These data suggest that it is possible to use 12geneΔ0HSR-iERG6 for genetic analyses (e. g., tetrad analysis).

4.9. The effect of AG1 derivatives on the multidrug hyper-sensitive strain 12geneΔ0HSR-iERG6

The effect of AG1 derivatives on yeast growth in liquid and on the plate (under glucose condition) were tested as described in the Materials and Methods sections. AG1 did not show toxicity against 12geneΔ0HSR-iERG6, but the highly active derivative O^7-propargyl AG1 showed toxicity on plate (Fig. 23A) and in liquid medium (Fig. 23B). These results show that it is possible to analyze the mode of action of O^7-propargyl AG1 using 12geneΔ0HSR-iERG6.

5. Conclusions and discussion

In this study, 12geneΔ0 was created by the disruption of 12 genes (eight ABC transporters on the plasma membrane and their four transcriptional factors) in strain BY4741. Strain 12geneΔ0 remained its mating and transformation efficiencies at levels comparable to those of BY4741, the parental strain. However, 12geneΔ0 showed decreased sporulation efficiency, a key property for genetics analyses. I therefore introduced the *RME1* (ins-308A) mutation to increase the sporulation efficiency, and created a strain, 12geneΔ0HSR. This strain showed multidrug sensitivity and high levels of sporulation efficiency comparable to those of BY4741. Interestingly, the physicochemical properties of the compounds to which 12geneΔ0HSR was showed improved sensitivities were fitted for the improved Lipinski's rule of five, the index for orally active drugs (Table 21, molecular weights ≤500, XLogP3 values ≤5, numbers of hydrogen bond donors ≤5 and numbers of hydrogen bond acceptors ≤10).[52] Therefore 12geneΔ0HSR strain will be useful not only for evaluation of mode of action of small molecules in genetic analyses, but also for screening for orally active lead compounds. Furthermore, the genetic interaction of ABC transporters and other genes was recently reported.[51] Therefore 12geneΔ0HSR will be a useful host strain to analyze the functions of single ABC transporters and genes which showed genetic interaction with ABC transporters because all ABC transporters of 12geneΔ0HSR on the plasma membrane are disrupted.

On the other hand, my finding revealed that the spectra of drug resistance between ABC

transporters and ergosterol are different, suggesting that ABC transporters and ergosterol confer drug resistance to different groups of compounds, and that *ERG6* gene is an important target for creating multidrug sensitive strain. In addition, 12geneΔ0HSR did not show sensitivities to AG1 or its derivatives.

I introduced the *ERG6* conditional expression system into 12geneΔ0HSR and created 12geneΔ0HSR-iERG6. This strain showed improved drug sensitivity to compounds for which resistance is shown by both ABC transporters and ergosterol. In addition, 12geneΔ0HSR-iERG6 showed sufficient transformation and sporulation efficiencies under the galactose condition. These results suggest that 12geneΔ0HSR-iERG6 can be used for genetic analysis and gene modifications. The strain 12geneΔ0HSR-iERG6 also showed O^7-propargyl AG1 sensitivity. It is thus possible to analyze the O^7-propargyl AG1-tubulin binding mode and the effects of O^7-propargyl AG1 on microtubules using 12geneΔ0HSR-iERG6.

There are previous analyses of microtubule inhibitors using yeast *in vivo* and *in vitro*. It was reported that human type mutations in the paclitaxel binding site (which binds β-tubulin and stabilize microtubule in mammalian cells) conferred paclitaxel sensitivity to *S. cerevisiae in vivo* and *in vitro*.[21] α-Tubulin was identified as a target of NKH-7, a cytotoxic 1-naphthol derivative compound by yeast genetic approach.[53] A screening of mutants using benomyl, a tubulin polymerization inhibitor, identified *bub*[54] and *mad*[55] genes, which are involved in mitotic and

spindle checkpoints in *S. cerevisiae*. In light of accumulated evidences, it appears that it will be possible to identify the important amino acids for the AG1 binding to the tubulin heterodimer and for the inhibition of microtubule dynamics by AG1 using PCR-based mutagenesis or spontaneous mutagenesis methods.

However there is variety on tubulin genes between human and yeast (e. g., 68% of homology between TUBB1 (human β-tubulin, UniProtKB/Swiss-Prot: Q9H4B7.1) and *TUB2* (yeast β-tubulin, NCBI Reference Sequence: NP_116616.1)), thus it is also expected that some tubulin inhibitors do not affect on yeast tubulin. In this case, the one way for analysis of tubulin inhibitors using yeast is expression of human type tubulin in 12geneΔ0HSR-iERG6. Using this strategy, I can analyze tubulin inhibitors by genetic analysis using 12geneΔ0HSR-iERG6.

In addition to yeast, a single-allele tubulin heterodimer is available from an insect cell expression and purification system.[56] In this system, it is possible to purify a single allele of α-tubulin and β-tubulin with specific post-translational modifications and to analyze the properties (e. g., the polymerization activity and the effect on kinesin-ATPase activity). These methods are useful to analyze microtubule inhibitor's effects at the single-allele and amino acid levels.

The 12geneΔ0HSR-iERG6 strain will also be useful for not only analyses of microtubule inhibitors but also chemical biology studies including the target identification of small compounds,[16] synthetic lethal/sick genetic interaction analyses,[57,58] genome-wide overexpression

screening,[23,59] haploinsufficiency-chemical sensitive assays[60] and more.

6. Figures and tables
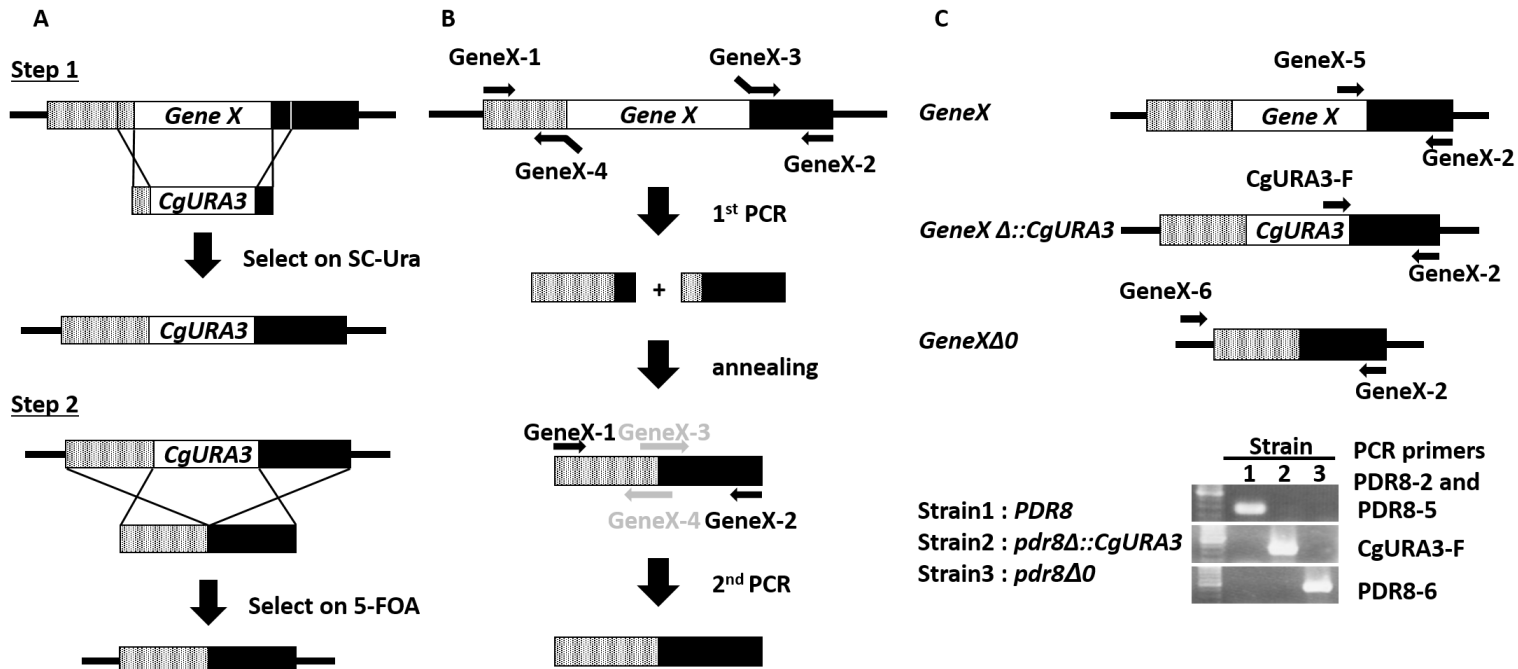
Fig. 14. The scheme of gene disruption.

A. Scheme of a modified PCR-based marker less gene disruption method.

After the deletion of *Gene X* by replacement with the *CgURA3* marker (Step 1), the *CgURA3* marker was popped out by the transformation of the DNA fragment which is directly ligated up- and down-stream of *Gene X* (Step 2).

B. Scheme of the construction of the DNA fragment which is directly ligated up- and down-stream of *Gene X*.

The 200 - 300 bp of 5'-UTR and 3'UTR fragments were amplified by PCR using Gene X-1/-4 and Gene X-2/-3 primers, respectively (1st PCR). These fragments were mixed and annealed (annealing step). Annealed fragments were amplified by the 2nd PCR using Gene X-1/-2 primers.

C. Confirmation of the constructed strain by colony direct PCR.

Primer "GeneX-6" (forward primer) anneals upstream (200 - 300 bp) of *GeneX*, primer "GeneX-2" (reverse primer) anneals downstream (200 - 300 bp) of *GeneX,* primer "GeneX-5" (forward primer) anneals the ORF of *GeneX,* and CgURA3-F（forward primer）anneals the ORF of *CgURA3* marker.
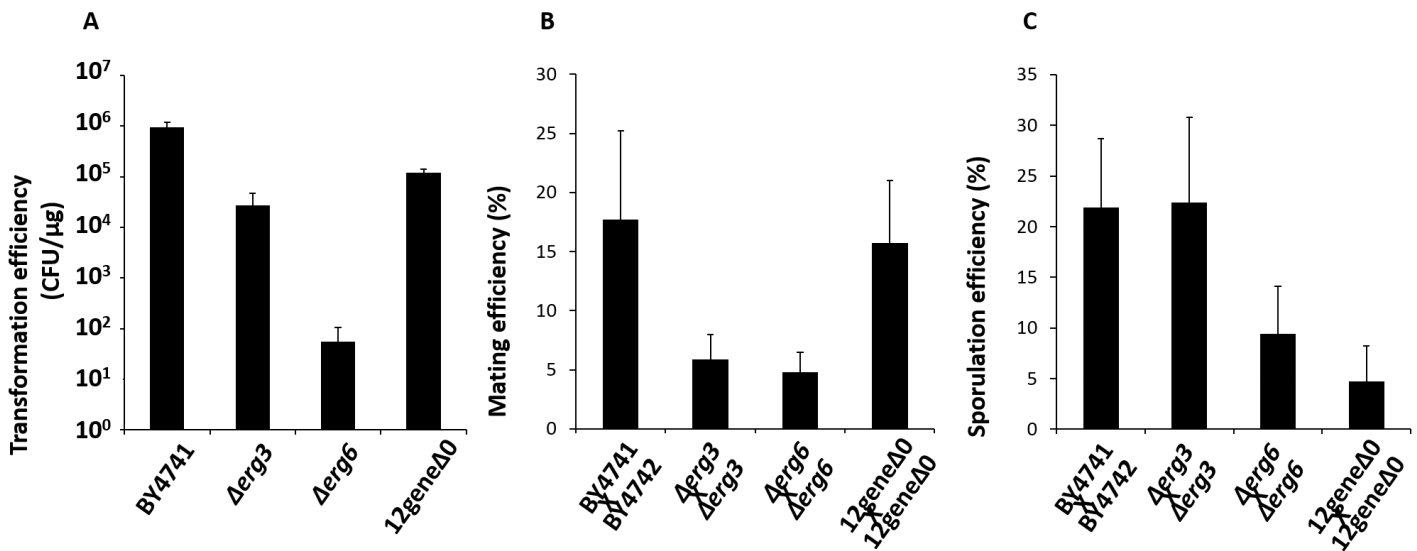
Fig. 15. Characterization of 12geneΔ0.

A. Transformation efficiency of 12geneΔ0.

One μg of pRS315 plasmid was transformed into each strains in the logarithmic growth phase (OD_{600} = 0.4, 20 mL). After selection on a SC-LEU plate, the numbers of colonies were counted, and colony forming units (cfu/μg) were calculated as the transformation efficiencies.

B. The mating efficiency of 12geneΔ0.

Each strains (*MATa* strain harboring pRS315 and *MATα* strains harboring pRS313) in the logarithmic growth phase were mixed and concentrated on a nitrocellulose membrane.

After incubation at 30ºC for 6 h, the cells were suspended in MilliQ and plated on the SC-LEU and SC-LEU/-HIS plates. After incubation at 30ºC for 2 - 3 days, mating efficiencies were calculated by dividing the number of colonies on SC-LEU/-HIS plate by on the SC-LEU plate.

C. The sporulation efficiency of 12geneΔ0.

The sporulation efficiencies of each strains were compared. Diploid cells of each strains were grown on a plate of sporulation medium at RT for 1 wk. The cells were observed under a microscope, and the percentage of cells with spores was calculated.
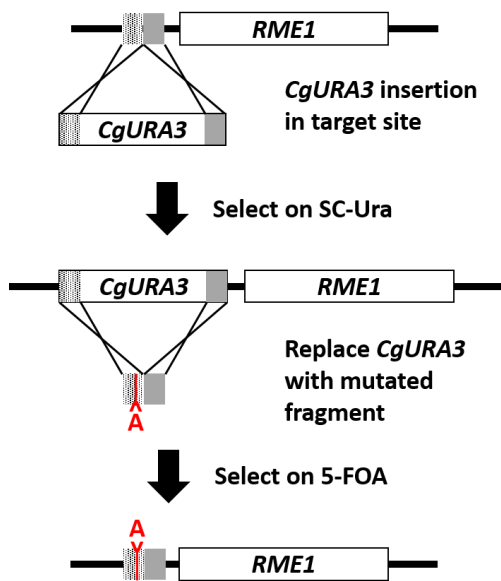
Fig. 16. The scheme of *RME1* (*ins-308A*) mutagenesis.

RME1 (*ins-308A*) mutagenesis was performed using the same scheme as the modified PCR-based marker less gene disruption method (Fig. 14).

CgURA3 marker was introduced in upstream of *RME1*. The *CgURA3* marker was then popped out by transformation of the DNA fragment which contains an adenine insertion 308 bp upstream from ATG of *RME1* (*ins-308A*).
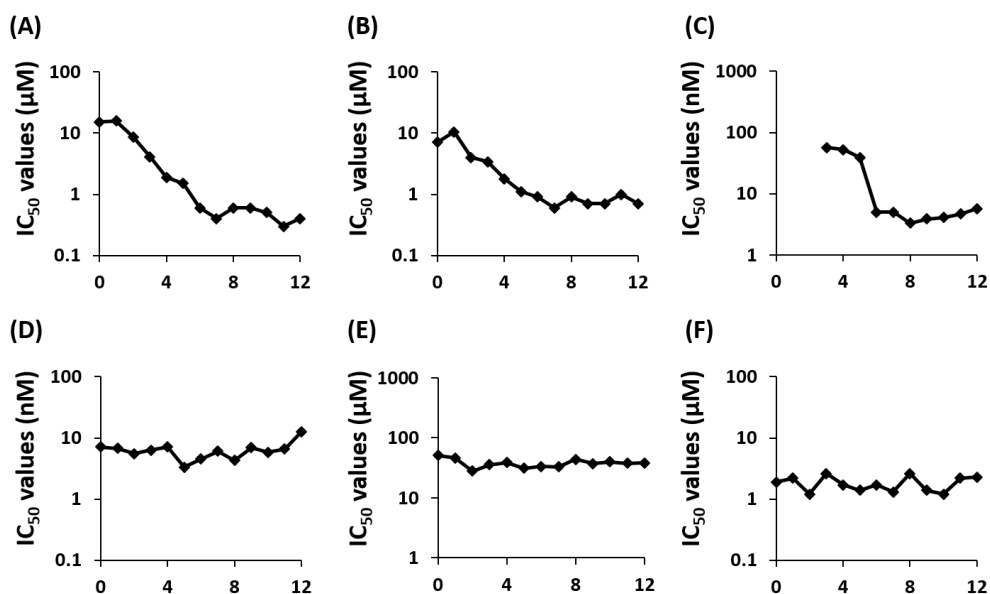
Fig. 17. Change of drug sensitivity with the number of deleted genes against several compounds.

Vertical axis indicates the IC_{50} values of each strains. And the number of horizontal axis indicates the number of deleted gene, that is, "0" means non deleted wild type strain BY4741. "1" and "2" means one- and two-gene deleted strains (1geneΔ0; *pdr3Δ0* and 2geneΔ0; *pdr3Δ0 pdr8Δ0* in Table 17), respectively, and so on. Tested compounds were (A) staurosporine, (B) 4-nitroquinoline 1-oxide, (C) latrunculin A, (D) rapamycin, (E) fluphenazine, and (F) digitonin.

Fig. 18. The effect AG1 derivatives on the growth of 12geneΔ0HSR.

The drug sensitivity of 12geneΔ0HSR was tested by halo assay. 12geneΔ0HSR was cultured in YPD liquid medium and diluted in 3 mL of 0.5% agar. Suspensions (the yeast cell number was adjusted at $OD_{600} = 0.05$) were poured onto YPD solid medium. Drug solutions were spotted on the plate containing each strains. After incubation for 3 days, the growth inhibition areas were compared. The drugs used were DMSO control (1), 15 nmole AG1 (2), and 15 nmole O^7-propargyl AG1 (3).
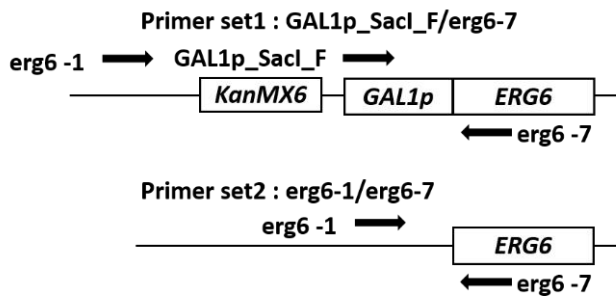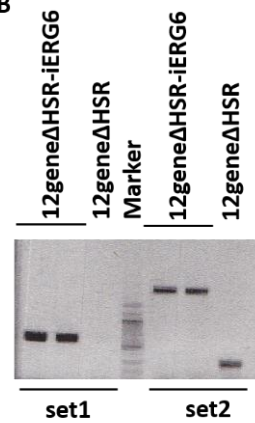
Fig. 19. The construction of 12geneΔ0HSR-iERG6.

A. The construction of 12geneΔ0HSR-iERG6 including primer annealing sites was as described.

B. The results of colony direct PCR (right part) of 12geneΔ0HSR-iERG6 showed that the PCR fragment was properly inserted in the 5'-UTR region of *ERG6*.
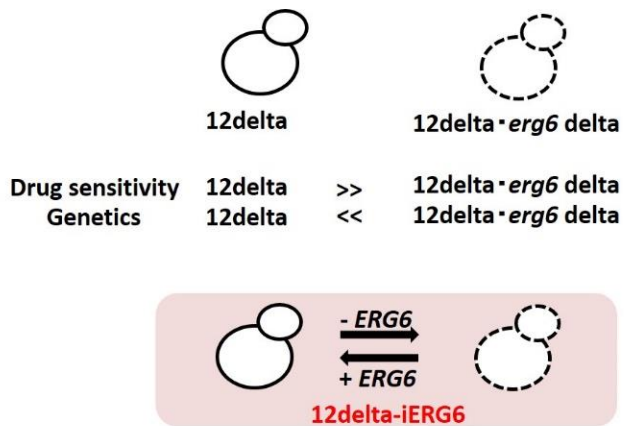
Fig. 20. The model of the *ERG6* conditional strain.

12geneΔ0HSR, ABC transporters disruptant, can be used for genetic analysis. On the other hand *ERG6* deletant in 12geneΔ0HSR can not be used for genetics, but this strain shows higher sensitivities than 12geneΔ0HSR to multiple drugs. Therefore, the *ERG6* conditional strain 12geneΔ0HSR-iERG6 will be useful tool for both drug testing and genetics.
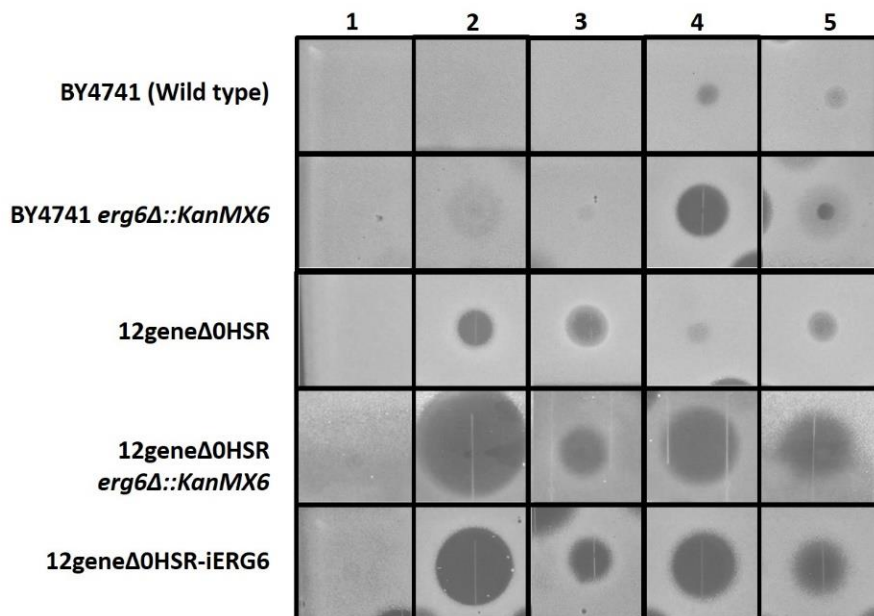
Fig. 21. The multidrug sensitivities of several yeast strains were tested by halo assay.

Strains were cultured in YPD liquid medium and diluted in 9 mL of 0.5% agar. The suspensions (the yeast cell density was adjusted at $OD_{600} = 0.05$) were poured onto YPD solid medium. Drug solutions were spotted on a plate containing each strains. After incubation for 3 days, the growth inhibition areas were compared. The drugs used were DMSO control (1), 1.5 nmole rhodamine 6G (2), 5 pmole latruncurin A (3), 50 nmole hygromycin B (4) and 15 nmole fluphenazine (5).
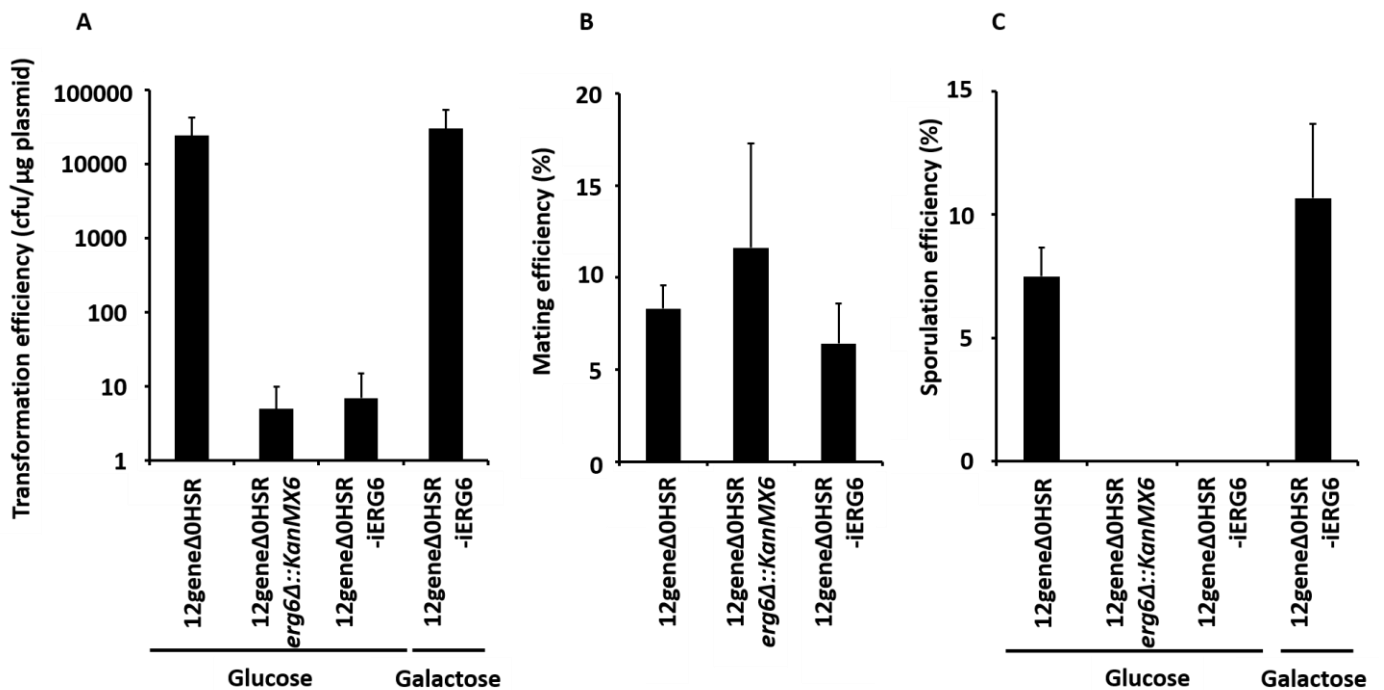
Fig. 22. Characterization of 12geneΔ0HSR-iERG6.

A. The transformation efficiency of 12geneΔ0HSR-iERG6.

One μg of pRS315 plasmid was transformed into each strain in the logarithmic growth phase (OD_{600} = 0.4, 20 mL). After selection on the SC-LEU plate, the numbers of colonies were counted, and colony forming units (cfu/μg) were calculated as the transformation efficiencies.

B. The mating efficiency of 12geneΔ0HSR-iERG6.

Each strains (*MATa* strain harboring pRS315 and *MATα* strains harboring pRS313) in the logarithmic growth phase were mixed and concentrated on a nitrocellulose membrane.

After incubation at 30ºC for 6 h, the cells were suspended in MilliQ and plated on SC-LEU and SC-LEU/-HIS plates. After incubation at 30ºC for 2 - 3 days, the mating efficiencies were calculated by dividing the number of colonies on the SC-LEU/-HIS plate by that on the SC-LEU plate.

C. The sporulation efficiency of 12geneΔ0HSR-iERG6.

The sporulation efficiencies of each strain were compared. Diploid cells of each strain were grown on a plate of sporulation medium at RT for 1 wk. Cells were observed under a microscope, and the percentage of cells with spores was calculated.
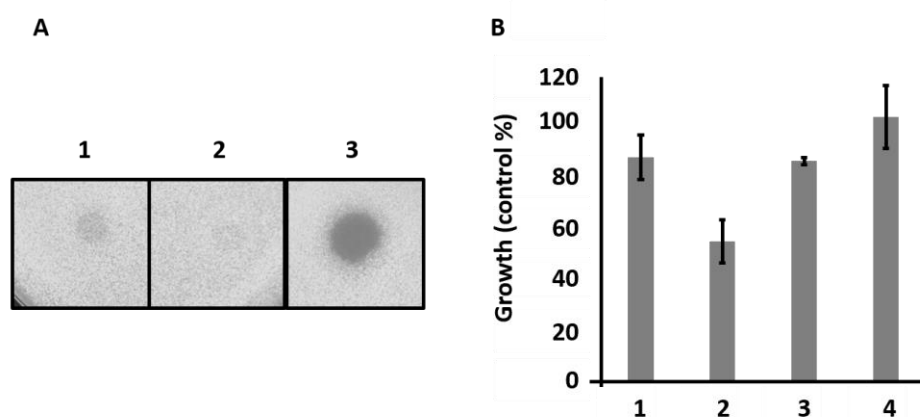
Fig. 23. The effect AG1 derivatives on the growth of 12geneΔ0HSR-iERG6.

A. The drug sensitivities of 12geneΔ0HSR-iERG6 were tested by halo assay. 12geneΔ0HSR-iERG6 was cultured in YPD liquid medium and diluted in 3 mL of 0.5% agar. The suspensions (the yeast cell number was adjusted at $OD_{600} = 0.05$) were poured onto YPD solid medium. Drug solutions were spotted on the plate containing each strains. After incubation for 3 days, the growth inhibition areas were compared. The drugs used were DMSO control (1), 15 nmole AG1 (2), and 15 nmole O^7-propargyl AG1 (3).

B. The drug sensitivity of 12geneΔ0HSR-iERG6 was tested by WST-8 assay. Cells ($OD_{600} = 0.1$) were treated with various concentrations of compounds. After incubation for 6 h in YPD liquid medium, the viability of the cells were measured using a cell-counting kit-8. The drugs used were 30 μM AG1 (1), 30 μM O^7-propargyl AG1 (2), 10 μM O^7-propargyl AG1 (3), and 3 μM O^7-propargyl AG1 (4).

Table 3. Primers

Name	Description
S1-PDR1	CTATTCATCTCAGCCAAGAATATACAGAAAGAATCCAAGAAACTGGAAGCGTACGCTGCAGGTCGAC
S2-PDR1	GGAAGGAAGTTTTTGAGAACTTTTATCTATACAAACGTATACGTTTAATCGATGAATTCGAGCTCG
S1-PDR3	GGCGACAACTGCATCAGCAGTTTTATTAATTTTTTCTTATTGCGTGACCGCACGTACGCTGCAGGTCGAC
S2-PDR3	GTCCCATTTACTATGGTTATGCTCTGCTTCCCTATTTCTTTTGCGTTTTCAATCGATGAATTCGAGCTCG
S1-PDR8	GTTGGTACGGGACGAATAAGAAAGAGGCAAACGGCACTTAGTTTGTTGGGCGTACGCTGCAGGTCGAC
S2-PDR8	GGGACGAAAAAATCCATGTAAAAAAATACATCAATCATAAATACATTTAATCGATGAATTCGAGCTCG
S1-YRR1	GAAAGTGGGAAAGTTTATTGCCCTCAGCCGTGCCAATAAGAATAGCGTCACACGTACGCTGCAGGTCGAC
S2-YRR1	AAAAAGGCTTCAAAGTAGTCGCGCCGCGAGATTGCCTCGACTTAGCATTAATCGATGAATTCGAGCTCG
S1-PDR5	CGTATCCGCTCGTTCGAAAGACTTTAGACAAAAatgCCCGAGGCCAAGCCGTACGCTGCAGGTCGAC
S2-PDR5	CCGTTCTTTTTAGGCACTCTTGCTAACCAGTAGAAAAAGACACCAGCGATCGATGAATTCGAGCTCG
S1-SNQ2	GTGGATAGAATAACACAGCTACCAAAATACGTAAAGAGAATTCAatgAGCCGTACGCTGCAGGTCGAC
S2-SNQ2	GGCAGATGAATGCACAAATGTTAAGTTATCTGAAGCCCACAttaCTGCATCGATGAATTCGAGCTCG
S1-YRS1	GATTAATATTACTGTTTTTATATTCAAAAGAGTAAAGCCGTTGCTATATACGAATCGTACGCTGCAGGTCGAC
S2-YRS1	CTGTTCTCGAAATCATTTTCCACAATACCAGATCTAGAACACATGCTTCTGATCGATGAATTCGAGCTCG
S1-PDR10	GGTCTTACATAGTTGTTAGGatgTTGCAAGCGCCCTCAAGTTCAAACTCGCGTACGCTGCAGGTCGAC
S2-PDR10	GGAACCCGCACCAGCCAGTATAAAAATATTGCTGCACAATAGTCAAAGACATCGATGAATTCGAGCTCG
S1-PDR11	GATGGGGCTACCGTTCAATTGGAAGAATCCCTCGGTGCTGTTCAGAAC

	GCGTACGCTGCAGGTCGAC
S2-PDR11	GGACCGCCTCATTGATGGGATACACTTCTTTATACCATCAATCACAGAAGATCGATGAATTCGAGCTCG
S1-PDR12	TTAAAAAAAGGTTTACAGATTTATTGTTATTGTTCTTATTAATAAAAAACGTACGCTGCAGGTCGAC
S2-PDR12	AAATTGTGTGTTAAACCACGAAATACAAATATATTTGCTTGCTTGTATCGATGAATTCGAGCTCG
S1-PDR15	CCTatgTCATCAGATATCAGAGACGTAGAGGAACGAAATTCGCGGAGCTCCGTACGCTGCAGGTCGAC
S2-PDR15	CGTCAtcaCTTCTTGGGTTTTTCGGAAATCTTACCGTTCTTCTTGGGTACATCGATGAATTCGAGCTCG
S1-AUS1	GTAATTCATCTCTCAGTCCTTGCAGTCTGCTTTTTCTGGAATTAATcgtacgctgcaggtcgac
S2-AUS1	AAAATTGCTATTAAGTAGAAGTAGAAATATATTTAAAAATGGTAatcgatgaattcgagctcg
PDR1-1	CAATAGCATGATAGCAGGACCATAGCGGC
PDR1-2	GAGAAGGAGATGCCCTAGAAAACAGAATG
PDR1-3	TATACAGAAAAGAATCCAAGAAACTGGAAGACGTATACGTTTGTATAGATAAAAGTTCTCAAAAAC
PDR1-4	GGAAGTTTTTGAGAACTTTTATCTATACAAACGTATACGTCTTCCAGTTTCTTGGATTCTTTTCTG
PDR1-5	CAACAGTAACAATTTTTCTGCAACTAG
PDR1-6	GAGTGGCAATAAGAGGCGC
PDR3-1	CTGCCGCTCGGACTTTCCGC
PDR3-2	GGACAGACTAAAGTTTCGCCC
PDR3-3	TTATTAATTTTTTCTTATTGCGTGACCGCAAAACGCAAAGAAATAGGGAAGCAGAGCATAACC
PDR3-4	CTATGGTTATGCTCTGCTTCCCTATTTCTTTTGCGTTTTGCGGTCACGCAATAAGAAAAAATTA
PDR3-5	CAACATTCTGCGCCTAGCCAAATAAGCGC
PDR3-6	CCTTGTTAACACCGTGCTC
PDR8-1	CGACAAGGTGCAATGCGG
PDR8-2	CCTCCTATCTGGCCGTTG
PDR8-3	GAAAGAGGCAAACGGCACTTAGTTTGTTGGGATGTATTTATGATTGATGTATTTTTTTACATGG

PDR8-4	CGAAAAAATCCATGTAAAAAATACATCAATCATAAATACATCCCAAC AAACTAAGTGCCGTTTGCC
PDR8-5	GATTGAAGATTTTATTAATGATGTTTGG
PDR8-6	CGCCAGAGGGTACAACAATG
YRR1-1	GGGGTAGAGGCTGATATACGGGG
YRR1-2	GGCGGTAAGCAGCGATTCAGC
YRR1-3	GCCCTCAGCCGTGCCAATAAGAATAGCGTCACATGCTAAGTCGAGGCA ATCTCGCGGCGCGACTAC
YRR1-4	CAAAGTAGTCGCGCCGCGAGATTGCCTCGACTTAGCATGTGACGCTAT TCTTATTGGCACGGCTG
YRR1-5	CAGAGATCATTCAGATGCTGACAGATG
YRR1-6	GAACGGAGTTAAATCCGCGG
PDR5-1	GCATAACCTTATGGCTGTTCGC
PDR5-2	CGCACCTATATGTAGTG
PDR5-3	CGTATCCGCTCGTTCGAAAGACTTTAGACTAGAATTTTGAATTTGGTTA AGAAAAGAAAC
PDR5-4	GGTAAGTTTCTTTTCTTAACCAAATTCAAAATTCTAGTCTAAAGTCTTT CGAACGAGCGG
PDR5-5	GTCAATTCTTTCTACAGTGAGAGATGGAG
PDR5-6	GAGAAATGTCTCCGCGGAAC
YRS1-1	GTGCCCTCTGAGTAGTGTCACGAAC
YRS1-2	CACACATAACTTTTTCTGCAAGTCATAG
YRS1-3	ATATACGAATTTTATATTATTTGTTGCATG
YRS1-4	ATAATATAAAATTCGTATATAGCAACGGCT
YRS1-5	GTGTATTGCTCACAGACTGAAGACC
YRS1-6	CGGAGGTAGAACAGCTCTCC
SNQ2-1	GAGTTCAAGCTCCCTGAGAAAACGAAGG
SNQ2-2	CGAGATGTACTCGTGTCTTCTTCTATAG
SNQ2-3	CAGCTACCAAAATACGTAAAGAGAATTCATGTGGGCTTCAGATAACTT AACATTTTGTGC
SNQ2-4	GATGAATGCACAAAATGTTAAGTTATCTGAAGCCCACATGAATTCTCT TTACGTATTTTGG
SNQ2-5	CATATCAGCTCTAAGTATAGCTACTTGTGG
SNQ2-6	GGAGTTACTATATCACCAGTGC
PDR10-1	GAAGGACGGTTGGGCAAGC

PDR10-2	GCAACATGGCGTAAACCTC
PDR10-3	CAATAATTTCTGGTCTTACATAGTTGTTAGGTTAAATATTACTGGCTACATTCATTGTATATGC
PDR10-4	CTAATTTTGCATATACAATGAATGTAGCCAGTAATATTTAACCTAACAACTATGTAAGACCAG
PDR10-5	CAGTTCTACCAATGATTATCTGGC
PDR10-6	CTACAGAATTGGTCGGC
PDR11-1	GTTCGTAAACGGGTTGG
PDR11-2	GAAGGCAGCCGGATGAGG
PDR11-3	CGATAGAGTAAAATTAGAGAAGCAACGCCTCGCGGTCAGTGAATAGCGTTCCGTTAGAAAAC
PDR11-4	CAATGTTTTCTAACGGAACGCTATTCACTGACCGCGAGGCGTTGCTTCTCTAATTTTACTC
PDR11-5	GCTTTAACATTGCCGCCATGTTTGTGGGC
PDR11-6	CCGCAGATCCTGCTCTCACC
PDR12-1	GGATAATCTGAAAAATAAACGG
PDR12-2	GATGTTAAAGGACGCCAAAATTTG
PDR12-3	TAATAAAAAACAAGCAAGCAAATATATTT
PDR12-4	GCTTGCTTGTTTTTTTATTAATAAGAACAATAAC
PDR12-5	GGGCCAAGAAAGGAAAGAC
PDR12-6	GGTAGTTCTCTTTTTGGGG
PDR15-1	GGAGCTCTCTACCTGGACC
PDR15-2	CTCCCCAGTAGAGAG
PDR15-3	CACACACACACACAAGCAAACACACTGACGTTATTTTCCTTTTTTTAGTTATATTATC
PDR15-4	AAAAGATAATATAACTAAAAAAAAGGAAAATAACGTCAGTGTGTTTGCTTGTGTGTGTG
PDR15-5	CTGCTATATTGCTTTTGATTATATCGCTGC
PDR15-6	CTGCTACTGCTGTGCGAG
AUS1-1	GCCTTAGTACCGTTTCTG
AUS1-2	GAGCGTCAGCGACAAGTATC
AUS1-3	TGGAATTAATTACCATTTTTAAATATATTT
AUS1-4	AAAAATGGTAATTAATTCCAGAAAAAGCAG
AUS1-5	GTAATTCCACACAGAGGG
AUS1-6	GACGGTGCCTTTGCCTTA

ADP1-1	GCGTCTTGAGTTGAAGTCAGG
ADP1-2	CAACGGGCAGTGGACCCTCTCG
ADP1-3	CAATTACAGTATAGGCGTCGTATATAGTCT
ADP1-4	CGACGCCTATACTGTAATTGCTTTTAGTT
ADP1-5	GACATCAAGATCCTGGCTCTG
ADP1-6	CCTCACTCTTTCCTTACTCACG
ERG6-2	GGTCGTTTGCCACGACATG
ERG6-5	CTAGAAAATGCTGCGGTTGG
CgURA3-F	GCTAATTCCGTTAAGAGAAGAGTCCTTCG
S1-ERG6	GTAGGCAGCATAAGATGAGTGAAACAGAATTGAGAAAAGACAGGCGTACGCTGCAGGTCGAC
S2-ERG6	ATCTTTTTATCTGCATATATAGGAAAATAGGTATATATCGTGCGCATCGATGAATTCGAGCTCG
S4-ERG6	AACTCCCTAGTGAATTGGGCCTGTCTTTTTCTCAATTCTGTTTCACTCATATAGGCCACTAGTGGATCTG
GAL1p_SacI_F	GGGAGCTCTAGTACGGATTAGA
GAL1p_EcoRI_R	GGGAATTCAATCCGGGGTTTTTTCTCCT
ERG6-1	CGGGTGTTTTCTCCTATCC
ERG6-2	GGTCGTTTGCCACGACATG
ERG6-7	GGGCAGAGTTGTTCTTCGAC
KanMX6-F	GGCCTGTTGAACAAGTCTGG

Table 4. Plasmids

Name	Description
pRS313	pBluescriptII-based yeast-*E.coli* shuttle vector containing *ARS*, centrosome sequence, and *HIS3* marker[61]
pRS315	pBluescriptII-based yeast-*E.coli* shuttle vector containing *ARS*, centrosome sequence, and *LEU2* marker[61]
pFA6a-*CgURA3*	Cassette vector for *CgURA3* marker[50]
pFA6a-*KanMX6*	Cassette vector for *KanMX6* marker[61]
pFA6a_*KanMX6*_pGAL1	Cassette vector for *KanMX6-Gal1p*[62]
pTC031	Cassette vector for *KanMX6-Gal1p*

Table 5. PCR mixture

Name	Concentration
pFA6a_*KanMX6*_pGAL1	10~1000 ng
Forward primer (GAL1p_SacI_F)	2　μM
Reverse primer (GAL1p_EcoRI_R)	2　μM
dNTPmix	200　μM
KOD dash buffer	1/10 dilution
KOD dash polymerase	0.025 U/μl

Table 6. PCR program

Temperature	Time	cycle
94ºC	4 min	x 1 cycle
94ºC	30 sec	x 30 cycles
54ºC	10 sec	
68ºC	30 sec	
72ºC	4 min	x 1 cycle

Table 7. Cassette PCR mixture

Name	Concentration
pFA6a-*CgURA3*, pFA6a-*KanMX6* or pTC031	10~1000 ng
Forward primer (S1-ERG6)	2　μM
Reverse primer (S2- or S4-ERG6)	2　μM
dNTPmix	200　μM
KOD dash buffer	1/10 dilution
KOD dash polymerase	0.025 U/μl

Table 8. Cassette PCR program

Temperature	time	cycle
97ºC	2 min	
97ºC	20 sec	x9 cycles
54ºC	30 sec	
68ºC	2 min10 sec	
97ºC	20 sec	x19 cycles
54ºC	30 sec	
68ºC	2 min10 sec (+20 sec/cycle)	

Table 9. 1st PCR mixture

Name	Concentration
BY4741 chromosome	10~1000 ng
Forward primer (GeneX-1 or -3)	2　μM
Reverse primer (GeneX-4 or -2)	2　μM
dNTPmix	200　μM
KOD dash buffer	1/10 dilution
KOD dash poly	0.025 U/μl

Table 10. 1st PCR program

Temperature	Time	cycle
94ºC	4 min	x 1 cycle
94ºC	30 sec	x 30 cycles
54ºC	10 sec	
68ºC	30 sec	
72ºC	4 min	x 1 cycle

Table 11. Annealing PCR mixture

Name	Concentration
1st PCR product	5 μl each
dNTPmix	200　μM
KOD dash buffer	1/10 dilution
KOD dash poly	0.025 U/μl

Table 12. Annealing PCR program

Temperature	Time	cycle
98ºC	30 sec	x 1 cycle
98ºC	10 sec	x 30 cycles
56ºC	20 sec	
72ºC	30 sec	

Table 13. 2nd PCR

Name	Concentration
annealing PCR product	20 μl
Forward primer (GeneX-1)	2 μM
Reverse primer (GeneX-2)	2 μM

Table 14. 2nd PCR program

Temperature	Time	cycle
98ºC	30 sec	x 1 cycle
98ºC	10 sec	x 30 cycles
54ºC	20 sec	
72ºC	40 sec	
72ºC	5 min	x 1 cycle

Table 15. Colony direct PCR mixture

Name	Concentration
Template	1 μl
Forward primer	2 μM
Reverse primer	2 μM
dNTPmix	200 μM
KOD dash buffer	1/10 dilution
KOD dash polymerase	0.025 U/μl

Table 16. Colony direct PCR program

Temperature	Time	cycle
94ºC	4 min	x 1 cycle
94ºC	30 sec	x 30 cycles
54ºC	10 sec	
68ºC	30 sec	
72ºC	4 min	x 1 cycle

Table 17. Constructed strains by multiple gene disruption

Strain	Relevant genotype
1geneΔ0	*MATa his3Δ1 leu2Δ0 met15Δ0 ura3Δ0 pdr3Δ0*
2geneΔ0	*MATa his3Δ1 leu2Δ0 met15Δ0 ura3Δ0 pdr3Δ0 pdr8Δ0*
3geneΔ0	*MATa his3Δ1 leu2Δ0 met15Δ0 ura3Δ0 pdr3Δ0 pdr8Δ0 pdr1Δ0*
4geneΔ0	*MATa his3Δ1 leu2Δ0 met15Δ0 ura3Δ0 pdr3Δ0 pdr8Δ0 pdr1Δ0 yrr1Δ0*
5geneΔ0	*MATa his3Δ1 leu2Δ0 met15Δ0 ura3Δ0 pdr3Δ0 pdr8Δ0 pdr1Δ0 yrr1Δ0 snq2Δ0*
6geneΔ0	*MATa his3Δ1 leu2Δ0 met15Δ0 ura3Δ0 pdr3Δ0 pdr8Δ0 pdr1Δ0 yrr1Δ0 snq2Δ0 pdr5Δ0*
7geneΔ0	*MATa his3Δ1 leu2Δ0 met15Δ0 ura3Δ0 pdr3Δ0 pdr8Δ0 pdr1Δ0 yrr1Δ0 snq2Δ0 pdr5Δ0 pdr10Δ0*
8geneΔ0	*MATa his3Δ1 leu2Δ0 met15Δ0 ura3Δ0 pdr3Δ0 pdr8Δ0 pdr1Δ0 yrr1Δ0 snq2Δ0 pdr5Δ0 pdr10Δ0 yor1Δ0*
9geneΔ0	*MATa his3Δ1 leu2Δ0 met15Δ0 ura3Δ0 pdr3Δ0 pdr8Δ0 pdr1Δ0 yrr1Δ0 snq2Δ0 pdr5Δ0 pdr10Δ0 yor1Δ0 pdr15Δ0*
10geneΔ0	*MATa his3Δ1 leu2Δ0 met15Δ0 ura3Δ0 pdr3Δ0 pdr8Δ0 pdr1Δ0 yrr1Δ0 snq2Δ0 pdr5Δ0 pdr10Δ0 yor1Δ0 pdr15Δ0 pdr11Δ0*
11geneΔ0	*MATa his3Δ1 leu2Δ0 met15Δ0 ura3Δ0 pdr3Δ0 pdr8Δ0 pdr1Δ0 yrr1Δ0 snq2Δ0 pdr5Δ0 pdr10Δ0 yor1Δ0 pdr15Δ0 pdr11Δ0 pdr12Δ0*
12geneΔ0	*MATa his3Δ1 leu2Δ0 met15Δ0 ura3Δ0 pdr3Δ0 pdr8Δ0 pdr1Δ0 yrr1Δ0 snq2Δ0 pdr5Δ0 pdr10Δ0 yor1Δ0 pdr15Δ0 pdr11Δ0 pdr12Δ0 aus1Δ0*

Table 18. Sporulation efficiency of *RME1* (ins-308A) and *MKT1* (D30G) mutants.

Strain	Sporulation efficiency[a] (% of spore-forming cells) (relative to WT/WT)
WT/WT diploid	21.9 ± 6.8 (1.0)
RME1(ins308A)/ RME1(ins308A)	48.8 ± 15.8 (2.2)
MKT1(D30G)/ MKT1(D30G)	51.7 ± 6.9 (2.4)
12geneΔ0/12geneΔ0 diploid	5.0 ± 2.9 (0.2)
RME1(ins308A)/ RME1(ins308A)	28.8 ± 4.6 (1.3)
MKT1(D30G)/ MKT1(D30G)	25.6 ± 5.9 (1.2)

Sporulation efficiencies and values relative to parental diploid cell (WT/WT). [a]Value ± SD.

Table 19. Drug sensitivities in the YPD liquid medium

Compound	IC$_{50}$ values			
	WT[a]	*erg3*[b]	*erg6*[c]	12geneΔ0HSR[d]
Anisomycin (μM)	> 37.7	28.5	5.8	8.5
Cycloheximide (nM)	268.3	30.5	8.0	30.6
Diamide (mM)	2.1	1.3	0.4	0.7
Digitonin (μM)	1.9	1.9	1.8	1.7
Fluconazole (μM)	> 100	> 100	> 100	4.1
Fluphenazine (μM)	51.1	44.5	4.0	43.6
G418 (μM)	72.4	42.2	9.1	51.0
Hygromycin B (μM)	238	36.8	8.6	92.0
Latruncurin A (nM)	> 237	162	> 237	4.8
Lovastatin (μM)	> 50	> 50	> 50	8.1
Manoalide (μM)	8.9	4.0	3.5	0.6
Menadione (mM)	0.7	0.6	0.7	0.5
4-Nitroquinoline 1-oxide (μM)	7.1	3.9	2.4	1.2
Nocodazole (μM)	> 100	> 100	> 100	5.1
Nystatin (μM)	0.5	1.2	3.8	0.6
Rapamycin (nM)	7.1	3.4	3.2	8.7
Rhodamine 6G (μM)	> 100	83.0	18.8	3.4
Staurosporine (μM)	15.1	2.2	1.4	0.2
Thiabendazole (μM)	304.7	247.2	157.6	541.9
Tunicamycin (μM)	308.6	258.2	645.2	159.4

IC^{50} value of constructed strains in the liquid were determined using WST-8 assay as described in Materials and Methods section. The strains used were [a]BY4741, [b]BY4741 *erg3Δ::CgURA3*, [c]BY4741 *erg6Δ::CgURA3* and [d]12geneΔ0HSR.

Table 20. Drug sensitivities in the YPD liquid medium (with glucose)

Compound	IC$_{50}$ values				
	BY4741	BY4741 erg6Δ[a]	12Δ[b]	12Δ erg6Δ[c]	12Δ -iERG6[d]
Fluconazole (μM)	70.8	6.7	1.4	0.8	1.0
Fluphenazine (μM)	57.1	8.6	21.1	5.8	3.9
Hygromycin B (μM)	109.8	6.3	111.9	4.7	4.6
Latruncurin A (nM)	659.0	176.2	4.2	1.7	1.9
Manoalide (μM)	17.1	5.8	1.6	0.5	0.4
Rhodamine 6G (μM)	>100.0	20.9	2.2	0.1	0.4

IC^{50} value of constructed strains in the liquid were determined using WST-8 assay as described in Materials and Methods section. The strains used were BY4741, [a]BY4741 *erg6Δ::KanMX6*, [b]12geneΔ0HSR, [c]12geneΔ0HSR *erg6Δ::KanMX6* and [d]12geneΔ0HSR-iERG6.

Table 21. Sensitivity fold and factors of "Rule of Five" of tested compounds.

Compound	Sensitivity fold[a]	Molecular weight	LogP[b]	H-Donor[c]	H-Acceptor[d]
Nystatin	0.8	926.1	-0.2	12	18
Rapamycin	0.8	914.2	6.0	3	13
Digitonin	1.1	1229.3	-3.9	17	29
Fluphenazine	1.2	437.5	4.4	1	7
G418	1.4	496.6	-5.8	10	14
Tunicamycin	1.9	718.7	-4.1	11	16
Hygromycin B	2.6	527.5	-6.6	11	16
Anisomycin	>4.4	265.3	0.9	2	5
4-Nitroquinoline 1-oxide	5.9	190.2	1.1	0	3
Lovastatin	>6.2	404.5	4.3	1	5
Cycloheximide	8.8	281.3	0.5	2	4
Manoalide	14.8	416.6	3.5	2	5
Nocodazole	>19.6	301.3	2.8	2	3
Fluconazole	>24.4	306.3	0.4	1	3
Rhodamine 6G	>29.4	443.6	5.1	2	4
Latrunculin A	>49.4	421.6	3.7	2	5
Staurosporine	75.5	466.5	3.2	2	4

[a]The values that IC_{50} of BY4741 was divided by that of 12geneΔ0HSR.

[b]XLogP3-AA values calculated by the algorithm[63]

[c]The number of hydrogen bond donors.

[d]The number of hydrogen bond acceptors.

CHAPTER 4. Concluding remark

In these experiment, I analyzed the effect of AG1 on the microtubule dynamics, and constructed multidrug hypersensitive yeast strain 12geneΔ0HSR-iERG6 for an investigation of the inhibitory mechanism of AG1.

In Chapter 2, it was revealed that AG1 binds to the colchicine site on the tubulin heterodimer and inhibits microtubule dynamics in mammalian cells. The inhibition of microtubule dynamics was caused mainly by the decrease of both the elongation and shortening velocities, and a decrease in the frequency of catastrophes. My analysis using AG1 revealed that microtubule dynamics in cells regulate the endosome transport and maturation, and that the inhibition of microtubule dynamics induces cell death in EGFR-overexpressing cells in an EGF-dependent manner. These results suggest that microtubule dynamics inhibitors kill cells *via* two pathways, the inhibition of mitotic spindle formation and the inhibition of endosome maturation. The present findings indicate that AG1 will be a useful tool to investigate the function of microtubule dynamics in cells.

In Chapter 3, I described the construction of the multidrug-sensitive strain 12geneΔ0HSR-iERG6 for analyzing the details of the mechanism of AG1's inhibition

of microtubule dynamics. 12geneΔ0HSR-iERG6 showed improved drug sensitivity to compounds including O^7-propargyl AG1. This strain showed sufficient transformation and sporulation efficiencies under the galactose condition. The results suggest that 12geneΔ0HSR-iERG6 is able to use for analysis of O^7-propargyl AG1. The analysis of O^7-propargyl AG1's effect on microtubule dynamics in greater detail using the 12geneΔ0HSR-iERG6 strain will provide new knowledge about the regulation of microtubule dynamics by inhibitors.

CHAPTER 5. Acknowledgements

I express my deep gratitude to all of the individuals who provided me guidance, support and encouragement during the preparation of this dissertation.

Most of all, I express my sincere thanks to Prof. Takeo Usui and Dr. Yoko Nagumo for their valuable guidance and encouragement, and Prof. Hiroshi Matsumoto, Prof. Toshiyuki Tanaka and Prof. Naoki Takaya for their critical advices for this Ph. D. thesis.

I also express my thanks to Prof. Hideo Kigoshi, Prof. Ichiro Hayakawa and Dr. Akiyuki Ikedo for the synthesis of AG1 and its derivatives, and Prof. Naoko Imamoto, Dr. Masatoshi Takagi, Dr. Hiroshi Masumoto and Mr. Yu Ota for their advices and technical supports.

I also express my thanks to my parents, members of Usui laboratory, Prof. Elmar Schiebel and members of Schiebel Laboratory and friends, especially Mr. Sora Enya, for their supports and encouragements.

Finally I express my deep gratitude to Japan Society for the Promotion Science for their financial supports.

CHAPTER 6. References

1) Kops, G. J., Weaver, B. A., and Cleve, D. W. (2005) On the road to cancer: aneuploidy and the mitotic checkpoint. *Nat. Rev. Cancer.* 5, 773-785.

2) Jackson, J.R., Patrick, D.R., Dar, M. M., and Huang, P.S. (2007) Targeted anti-mitotic therapies: can we improve on tubulin agents? *Nat. Rev. Cancer* 7, 107-117.

3) Dumontet, C., and Jordan, M. A. (2010) Microtubule-binding agents: a dynamic field of cancer therapeutics. *Nat. Rev. Drug Des*. 9, 790-803.

4) Howard, J., and Hyman, A. A. (2009) Growth, fluctuation and switching at microtubule plus ends. *Nat. Rev. Mol. Cell Biol.* 10, 569-574.

5) Towle, M. J., Salvato, K. A., Budrow, J., Wels, B. F., Kuznetsov, G., Aalfs, K. K., Welsh, S., Zheng, W., Seletsky, B. M., Palme, M. H., Habgood, G. J., Singer, L. A., Dipietro, L. V., Wang, Y., Chen, J. J., Quincy, D. A., Davis, A., Yoshimatsu, K., Kishi, Y., Yu, M. J., and Littlefield, B. A. (2001) In vitro and in vivo anticancer activities of synthetic macrocyclic ketone analogues of halichondrin B. *Cancer Res*. 61, 1013−1021.

6) Pean, E., Klaar, S., Berglund, E. G., Salmonson, T., Borregaard, J., Hofland,

K. F., Ersbøll, J., Abadie, E., Giuliani, R., and Pignatti, F. (2012) The European medicines agency review of eribulin for the treatment of patients with locally advanced or metastatic breast cancer: summary of the scientific assessment of the committee for medicinal products for human use. *Clin Cancer Res.* 18, 4491-4497.

7) U.S. Food and Drug Administration on HALAVEN[TM] (eribulin mesylate) Injection. U.S. Food and Drug Administration. http://www.access-data.fda.gov/drugsatfda_docs/label/2010/201532lbl.pdf. Accessed January 4th, 2013.

8) Hattori, M., Fujita, T., Sawaki, M., Kondo, N., Horio, A., Ushio, A., Gondo, N., Idota, A., Ichikawa, M., and Iwata, H. (2013) [Clinical efficacy and safety assessment of eribulin monotherapy in patients with metastatic breast cancer - a single- institute experience] *Gan To Kagaku Ryoho* 40, 737-741.

9) Jordan, M. A., Kamath, K., Manna, T., Okouneva, T., Miller, H. P., Davis, C., Littlefield, B. A., and Wilson, L. (2005) The primary antimitotic mechanism of action of the synthetic halichondrin E7389 is suppression of microtubule growth. *Mol. Cancer Ther.* 4, 1086−1095.

10) Smith, J. A., Wilson, L., Azarenko, O., Zhu, X., Lewis, B. M., Littlefield, B.

A., and Jordan, M. A. (2010) Eribulin binds at microtubule ends to a single site on tubulin to suppress dynamic instability. *Biochemistry* 49, 1331−1337.

11) Yokosuka, A., Haraguchi, M., Usui, T., Kazami, S., Osada, H., Yamori, T., and Mimaki, Y. (2007) Glaziovianin A, a new isoflavone, from the leaves of Ateleia glazioviana and its cytotoxic activity against human cancer cells. *Bioorg. Med. Chem. Lett.* 17, 3091-3094.

12) Schuyler, S. C. and Pellman, D. (2001) Microtubule "plus-end-tracking proteins": The end is just the beginning. *Cell* 105, 421-424.

13) Salaycik, K. J., Fragerstrom, C. J., Murthy K., Tulu U. S., and Wadsworth P. (2005) Quantification of microtubule nucleation, growth and dynamics in wound-edge cells. *J. Cell Sci.* 118, 4113-4122.

14) Usui, T., Kazami, S., Dohmae, N., Mashimo, Y., Kondo, H., Tsuda, M., Terasaki, G. A., Ohashi, K., Kobayashi, J., and Osada, H. (2004) Amphidinolide H, a potent cytotoxic macrolide, covalently binds on actin subdomain 4 and stabilizes actin filament. *Chem. Biol.* 11, 1269-1277.

15) Chinen, T., Kazami, S., Nagumo, Y., Hayakawa, I., Ikedo, A., Takagi, M., Yokosuka, A., Imamoto, N., Mimaki, Y., Kigoshi, H., Osada, H., and Usui, T. (2013) Glaziovianin A prevents endosome maturation via inhibiting

microtubule dynamics. *ACS Chem Biol.* 8, 884-889.

16) Miyamoto, Y., Machida, K., Mizunuma, M., Emoto, Y., Sato, N., Miyahara, K., Hirata, D., Usui, T., Takahashi, H., Osada, H., and Miyakawa, T. (2002) Identification of Saccharomyces cerevisiae isoleucyl-tRNA synthetase as a target of the G1-specific inhibitor Reveromycin A. *J. Biol. Chem.* 277, 28810-28814.

17) Kazami, S., Muroi, M., Kawatani, M., Kubota, T., Usui, T., Kobayashi, J., and Osada, H. (2006) Iejimalides shows anti-osteoclast activity via V-ATPase inhibition. *Biosci. Biotechnol. Biochem.* 70, 1364-1370.

18) Janke C., and Bulinski, J. C. (2011) Post-translational regulation of the microtubule cytoskeleton: mechanisms and functions. *Nat. Rev. Mol. Cell Biol.* 12, 773-786.

19) Li, J., Katiyar, S. K., and Edlind, T. D. (1996) Site-directed mutagenesis of Saccharomyces cerevisiae beta-tubulin: interaction between residue 167 and benzimidazole compounds. *FEBS Lett.* 385, 7-10.

20) Schatz, P. J., Solomon, F., and Botstein, D., (1986) Genetically essential and nonessential alpha-tubulin genes specify functionally interchangeable proteins. *Mol. Cell Biol.,* 6, 3722-3733.

21) Gupta, M. L. Jr, Bode, C. J., Georg, G. I., and Himes, R. H. (2003) Understanding tubulin-Taxol interactions: mutations that impart Taxol binding to yeast tubulin. *Proc. Natl. Acad. Sci. U S A*. 100, 6394-6397.

22) Foland, T. B., Dentler, W. L., Suprenant, K. A., Gupta, M. L. Jr, and Himes, R. H. (2005) Paclitaxel-induced microtubule stabilization causes mitotic block and apoptotic-like cell death in a paclitaxel-sensitive strain of Saccharomyces cerevisiae. *Yeast* 22, 971-978.

23) Arita, Y., Nishimura, S., Matsuyama, A., Yashiroda, Y., Usui, T., Boone, C., and Yoshida, M. (2011) Microarray-based target identification using drug hypersensitive fission yeast expressing ORFeome. *Mol. Biosyst.* 7, 1463-1472.

24) Decottignies, A., and Goffeau, A. (1997) Complete inventory of the yeast ABC proteins. *Nat. Genet.* 15, 137-145.

25) Bauer, B. E., Wolfger, H., and Kuchker, K. (1997) Inventory and function of yeast ABC proteins: about sex, stress, pleiotropic drug and heavy metal resistance. *Biochim. Biophys. Acta.* 1461, 217-236.

26) Jungwirth, H., and Kuchler, K. (2006) Yeast ABC transporters-- a tale of sex,

stress, drugs and aging. *FEBS Lett.* 580, 1131-1138.

27) Simon, J. A., and Bedalov, A. (2004) Yeast as a model system for anticancer drug discovery. *Nat. Rev. Cancer* 4, 481-492.

28) Ravelli, R. B., Gigant, B., Curmi, P. A., Jourdain, I., Lachkar, S., Sobel, A., and Knossow M. (2004) Insight into tubulin regulation from a complex with colchicine and a stathmin-like domain. *Nature* 428, 198-202.

29) Gigant, B., Wang, C., Ravelli, R. B., Roussi, F., Steinmetz, M. O., Curmi, P. A., Sobel, A., and Knossow, M. (2005) Structural basis for the regulation of tubulin by vinblastine. *Nature* 435, 519-522.

30) Kitano, M., Nakaya, M., Nakamura, T., Nagata, S., and Matsuda, M. (2008) Imaging of Rab5 activity identifies essential regulators for phagosome maturation. *Nature* 453, 241-245.

31) Kapoor, S., and Panda, D. (2012) Kinetic stabilization of microtubule dynamics by indanocine perturbs EB1 localization, induces defects in cell polarity and inhibits migration of MDA-MB-231 cells. *Biochem Pharmacol.* 83, 1495-1506.

32) Li, H., Daun, Z. W., Xie, P., Liu, Y. R., Wang, W. C., Dou, S. X., and Wang, P. Y. (2012) Effects of paclitaxel on EGFR endocytic trafficking revealed using

quantum dot tracking in single cells. *PLoS One* e45465.

33) Yvon, A. M., Wadsworth, P., and Jordan, M. A. (1999) Taxol suppresses dynamics of individual microtubules in living human tumor cells. *Mol. Biol. Cell.* 10, 947-959.

34) Hayakawa, I., Ikedo, A., Chinen, T., Usui, T., and Kigoshi, H. (2012) Design, synthesis, and biological evaluation of the analogues of glaziovianin A, a potent antitumor isoflavone. *Bioorg Med Chem.* 20, 5745-5756.

35) Castoldi, M., and Popov, A. V. (2003) Purification of brain tubulin through two cycles of polymerization-depolymerization in a high-molarity buffer. *Protein Expression Purif.* 32, 83−88.

36) Kondoh, M., Usui, T., Nishikiori, T., Mayumi, T., and Osada, H. (1999) Apoptosis induction via microtubule disassembly by an antitumour compound, pironetin. *Biochem. J.* 340, 411-416

37) Yamazaki, Y., Tanaka, K., Nicholson, B., Deyanat-Yazdi, G., Potts, B., Yoshida, T., Oda, A., Kitagawa, T., Orikasa, S., Kiso, Y., Yasui, H., Akamatsu, M., Chinen, T., Usui, T., Shinozaki, Y., Yakushiji, F., Miller, B. R., Neuteboom, S., Palladino, M., Kanoh, K., Lloyd, G. K., and Hayashi, Y. (2012) Synthesis and structure-activity relationship study of antimicrotubule

agents phenylahistin derivatives with a didehydropiperazine-2,5-dione structure. *J. Med. Chem.* 55, 1056-1071.

38) Yamazaki, Y., Sumikura, M., Masuda, Y., Hayashi, Y., Yasui, H., Kiso, Y., Chinen, T., Usui, T., Yakushiji, F., Potts, B., Neuteboom, S., Palladino, M., Lloyd, G. K., and Hayashi, Y. (2012) Synthesis and structure-activity relationships of benzophenone-bearing diketopiperazine-type anti-microtubule agents. *Bioorg Med. Chem.* 20, 4279-4289.

39) Gierke, S., Kumar, P., and Wittmann, T. (2010) Analysis of microtubule polymerization dynamics in live cells. *Methods Cell Biol.* 97, 15−33.

40) Landen, J. W., Lang, R., McMahon, S. J., Rusan, N. M., Yvon, A. M., Adams, A. W., Sorcinelli, M. D., Campbell, R., Bonaccorsi, P., Ansel, J. C., Archer, D. R., Wadsworth, P., Armstrong, C. A., and Joshi, H. C. (2002) Noscapine alters microtubule dynamics in living cells and inhibits the progression of melanoma. *Cancer Res.* 62, 4109−4114.

41) Tomas, A., Futter, C. E., and Eden, E. R. (2014) EGF receptor trafficking: consequences for signaling and cancer. *Trends Cell Biol.* 24, 26-34.

42) Zhang, Y., Wang, L., Zhang, M., Jin, M., Bai, C., and Wang, X. (2012) Potential mechanism of interleukin-8 production from lung cancer cells: an

involvement of EGF-EGFR-PI3K-Akt-Erk pathway. *J. Cell Physiol.* 227, 35-43.

43) Yoshimoto, Y., and Imoto, M. (2002) Induction of EGF-dependent apoptosis by vacuolar-type H (+)-ATPase inhibitors in A431 cells overexpressing the EGF receptor. *Exp. Cell Res.* 279, 118-127.

44) Rush, J. S., Quinalty, L. M., Engelman, L., Sherry, D. M., and Ceresa, B. P. (2012) Endosomal accumulation of the activated epidermal growth factor receptor (EGFR) induces apoptosis. *J. Biol. Chem.* 287, 712-722.

45) Brachmann, C. B., Davies, A., Cost, G. J., Caputo, E., Li, J., Hieter, P., and Boeke, J. D. (1998) Designer deletion strains derived from Saccharomyces cerevisiae S288C: a useful set of strains and plasmids for PCR-mediated gene disruption and other applications. *Yeast* 14, 115-132.

46) Herskowitz, I., Jensen, R. E. (1991) Putting the HO gene to work: practical uses for mating-type switching. *Methods Enzymol.* 194, 132-146.

47) Storici, F., Lewis, L. K., and Resnick, M. A. (2001) In vivo site-directed mutagenesis using oligonucleotides. *Nat Biotechnol.* 19, 773-776.

48) Deutschbauer, A. M., and Davis, R. W. (2005) Quantitative trait loci mapped to single-nucleotide resolution in yeast. *Nat Genet.* 37, 1333-1340.

49) Dimitrov, L. N., Brem, R. B., Kruglyak, L., and Gottschling, D. E. (2009) Polymorphisms in multiple genes contribute to the spontaneous mitochondrial genome instability of Saccharomyces cerevisiae S288C strains. *Genetics* 183, 365-383.

50) Chinen, T., Ota, Y., Nagumo, Y., Masumoto, H., and Usui, T. (2011) Construction of multidrug-sensitive yeast with high sporulation efficiency. *Biosci. Biotechnol. Biochem.* 75, 1588-1593.

51) Snider, J., Hanif, A., Lee, M. E., Jin, K., Yu, A. R., Graham, C., Chuk, M., Damjanovic, D., Wierzbicka, M., Tang, P., Balderes, D., Wong, V., Jessulat, M., Darowski, K. D., San Luis, B. J., Shevelev, I., Sturley, S. L., Boone, C., Greenblatt, J. F., Zhang, Z., Paumi, C. M., Babu, M., Park, H. O., Michaelis, S., and Stagljar, I. (2013) Mapping the functional yeast ABC transporter interactome. *Nat. Chem. Biol.* 9, 565-572.

52) Lipinski, C. A., Lombardo, F., Dominy, B. W., and Feeney, P. J. (2001) Experimental and computational approaches to estimate solubility and permeability in drug discovery and development settings. *Adv. Drug Deliv. Rev.* 46, 3-26.

53) Chanklan, R., Mizunuma, M., Kongkathip, N., Hasitapan, K., Kongkathip, B.,

Miyakawa, T. (2008) Identification of Saccharomyces cerevisiae Tub1 alpha-tubulin as a potential target for NKH-7, a cytotoxic 1-naphthol derivative compound. *Biosci Biotechnol Biochem.* 72, 19-27.

54) Hoyt, M. A., Totis, L, and Roberts, B. T. (1991) *S. cerevisiae* genes required for cell cycle arrest in response to loss of microtubule function. *Cell* 66, 507-517.

55) Li, R., and Murray, A. W. (1991) Feedback control of mitosis in budding yeast. *Cell* 66, 519-531.

56) Minoura, I., Hachikubo, Y., Yamakita, Y., Takazaki, H., Ayukawa, R., Uchimura, S., and Muto, E. (2013) Overexpression, purification, and functional analysis of recombinant human tubulin dimer. *FEBS Lett.* 587, 450-455.

57) Tong, A. H., Evangelista, M., Parsons, A. B., Xu, H., Bader, G. D., Pagé, N., Robinson, M., Raghibizadeh, S., Hogue, C. W., Bussey, H., Andrews, B., Tyers, M., and Boone, C. (2001) Systematic genetic analysis with ordered arrays of yeast deletion mutants. *Science* 294, 2364-2368.

58) Parsons, A. B., Brost, R. L., Ding, H., Li Z., Zhang, C., Sheikh, B., Brown, G. W., Kane, P. M., Hughes, T. R., and Boone, C. (2004) Integration of

chemical-genetic and genetic interaction data links bioactive compounds to cellular target pathways. *Nat Biotechnol*. 22, 62-69.

59) Nishimura, S., Arita, Y., Honda, M., Iwamoto, K., Matsuyama, A., Shirai, A., Kawasaki, H., Kakeya, H., Kobayashi, T., Matsunaga, S., and Yoshida, M. (2010) Marine antifungal theonellamides target 3beta-hydroxysterol to activate Rho1 signaling. *Nat Chem Biol.* 6, 519-526.

60) Giaever, G., Shoemaker, D. D., Jones, T. W., Liang, H., Winzeler, E. A., Astromoff, A., and Davis, R. W. (1999) Genomic profiling of drug sensitivities via induced haploinsufficiency. *Nat. Genet.* 21, 278-283.

61) Sikorski, R. S. and Hieter, P. (1989) A system of shuttle vectors and yeast host strains designed for efficient manipulation of DNA in Saccharomyces cerevisiae. *Genetics* 122, 19-27.

62) Bahler, J., Wu J. Q., Longtine, M. S., Shah, N. G., McKenzie, A. 3rd, Steever, A. B., Wach, A., Philippsen, P., and Pringle, J. R. (1998) Heterologous modules for efficient and versatile PCR-based gene targeting in Schizosaccharomyces pombe. *Yeast* 14, 943-951.

63) Cheng, T., Zhao, Y., Li, X., Lin, F., Xu, Y., Zhang, X., Li, Y., Wang, R., Lai, L. (2007) Computation of octanol-water partition coefficients by guiding an

additive model with knowledge. *J. Chem. Inf. Model.* 47, 2140-2148.

CHAPTER 7. Supplements

Supplement 1   Antibody, fluorescent probe and ^{3}H-labeled compounds

Name	Concentration	Manufacture Description
Fluorescent probe		
DAPI	0.1 μg/ml	Dojindo (340-07971)
Alexa^{488} conjugated EGF	1 μg/ml	Life technologies (Cat# E13345)
Alexa^{488} conjugated anti-mouce IgG	1 : 2000	Invitrogen (Cat# A11001)
Alexa^{568} conjugated anti-rabbit IgG	1 : 2000	Invitrogen (Cat# A11011)
Primary antibodies		
anti-EGFR	1 : 1000 (WB) 1 : 250 (IF)	Santa Cruz (Cat# sc-03)
anti-Phospho-EGFR (pY1068)	1 : 2000 (WB)	Cell signaling (Cat# 3777)
anti-ERK	1 : 5000 (WB)	BD bioscience (Cat# 610030)
anti-Phospho-ERK (pT202/pY204)	1 : 1000 (WB)	BD bioscience (Cat# 612358)
anti-β-actin		Abcam (Cat# ab8227-50)
anti-α-tubulin (DM1A)	1 : 1000 1 : 250 (IF)	Santa Cruz (Cat# sc-32293)
Secondary antibodies		
HRP-conjugated anti-rabbit	1 : 3000	KPL (Cat# 474-1506)
HRP-conjugated anti-mouse	1 : 3000	KPL (Cat # 474-1806)
Radio isotope compound		
Colchicine, [ring C, methoxy-^{3}H]- (85.3 Ci/mmol)	50 nM	Perkin Elmer (Cat# NET189250UC)
Vinblastine sulfate, [^{3}H]- (2 Ci/mmol)	50 nM	Moravek Biochemicals, Inc. (Cat# MT-657S)

Supplement 2   DMEM containing 10% FCS

Name	Concentration		Manufacture Description
DMEM	88	%	Nacalai Tesque (Cat# 08458-74)
Penicillin Streptomycin solution	1	%	Nacalai Tesque (Cat# 26253-84)
Fetal calf serum (FCS)	10	%	Cell Culture Bioscience (Cat# 171012, Lot# 8G0297)

Supplement 3   DMEM without FCS

Name	Concentration		Manufacture Description
DMEM	99	%	Nacalai Tesque (Cat# 08458-74)
Penicillin Streptomycin solution	1	%	Nacalai Tesque (Cat# 26253-84)

Supplement 4   RB buffer

Name	Concentration	Manufacture Description
MES (pH6.8)	100 mM	Dojindo (Cat# 349-01623)
$MgCl_2$	0.5 mM	Nacalai Tesque (Cat# 20909-42)
EGTA	1 mM	Dojindo (Cat# 342-01314)

Supplement 5   Phosphate Buffer Saline (PBS)

Name	Concentration		Manufacture Description
NaCl	137	mM	Wako (Cat# 198-01675)
Na_2HPO_4	8.1	mM	Wako (Cat# 196-02835)
KCl	2.68	mM	Wako (Cat# 163-03545)
NaH_2PO_4	1.48	mM	Wako (Cat# 192-02815)

Supplement 6   Sodium Lauryl sulfate (SDS) sample buffer

Name	Concentration		Manufacture Description
Tris-HCl (pH6.8)	62.5	mM	Nacalai Tesque (Cat# 35434-34)
Sodium lauryl sulfate (SDS)	2	%	Nacalai Tesque (Cat# 08933-05)
Glycerol	10	%	Nacalai Tesque (Cat# 17018-83)
β-Mercaptoethanol	5	%	Nacalai Tesque (Cat# 21438-83)

Supplement 7   YPD medium

Name	Concentration		Manufacture Description
Yeast Extract	1	%	Nacalai Tesque (Cat# 15838-45)
Polypeptone	2	%	Wako (Cat# 394-00115)
Glucose	2	%	Nacalai Tesque (Cat# 16806-25)

Supplement 8   Amino acid mix

Name	Concentration		Manufacture Description
L-Alanine	2	g	Wako (Cat# 010-01042)
Adenine	2	g	Wako (Cat# 013-00812)
L-Arginine	2	g	Wako (Cat# 017-04612)
L-Asparagine	2	g	Wako (Cat# 019-04812)
L-Aspartic acid	2	g	Wako (Cat# 013-04832)
L-Cysteine	2	g	Nacalai Tesque (Cat# 10309-12)
L-Glutamine	2	g	Wako (Cat# 074-00522)
L-Glutamic acid	2	g	Wako (Cat# 16911-35)
Glycin	2	g	Wako (Cat# 073-00732)
L-Histidine	2	g	Wako (Cat# 084-00682)
myo-Inositol	2	g	Wako (Cat# 092-00282)
L-Isoleucine	2	g	Wako (Cat# 121-00862)
L-Leucine	4	g	Wako (Cat# 124-00852)
L-Lysine	2	g	Wako (Cat# 124-01452)
L-Methionine	2	g	Wako (Cat# 133-01602)
p-Aminobenzonic acid	0.2	g	Wako (Cat# 015-02332)
L-Phenylalanine	2	g	Wako (Cat# 161-01302)
L-Proline	2	g	Wako (Cat# 161-04602)
L-Serine	2	g	Wako (Cat# 199-00402)
L-Threonine	2	g	Wako (Cat# 204-01322)
L-Tryptophan	2	g	Nacalai Tesque (Cat# 35607-32)
L-Tyrosine	2	g	Wako (Cat# 202-03562)
Uracil	2	g	Wako (Cat# 212-00062)
L-Valine	2	g	Wako (Cat# 228-00082)

Supplement 9 SC-LEU medium

Name	Concentration		Manufacture Description
Yeast nitrogen base without amino acid	0.67	%	BD Bioscience (Cat# BD291940)
Amino acid mix without leucine (Supplement 8)	0.2	%	
Glucose	2	%	Nacalai Tesque (Cat# 16806-25)

Supplement 10 SC-HIS medium

Name	Concentration		Manufacture Description
Yeast nitrogen base without amino acid	0.67	%	BD Bioscience (Cat# BD291940)
Amino acid mix without histidine (Supplement 8)	0.2	%	
Glucose	2	%	Nacalai Tesque (Cat# 16806-25)

Supplement 11 SC-LEU/-HIS medium

Name	Concentration		Manufacture Description
Yeast nitrogen base without amino acid	0.67	%	BD Bioscience (Cat# BD291940)
Amino acid mix without leucine and histidine (Supplement 8)	0.2	%	
Glucose	2	%	Nacalai Tesque (Cat# 16806-25)

Supplement 12 5-FOA medium

Name	Concentration		Manufacture Description
Yeast nitrogen base without amino acid	0.67	%	BD Bioscience Cat# 2015-11-30)
Amino acid mix (Supplement 8)	0.2	%	
Glucose	2	%	Nacalai Tesque (Cat#16806-25)
5-Fluoroorotic acid (5-FOA)	0.1	%	Wako (Cat# 060-04923)

Supplement 13 YP-Raf/Gal medium

Name	Concentration		Manufacture Description
Yeast Extract	1	%	Nacalai Tesque (Cat# 15838-45)
Polypeptone	2	%	Wako (Cat# 394-00115)
Raffinose	3	%	Sigma (Cat# R0250)
Galactose	2	%	Sigma (Cat# G0750)

Supplement 14 Pre-sporulation medium (Glucose)

Name	Concentration		Manufacture Description
Yeast extract	0.8	%	Nacalai Tesque (Cat# 15838-45)
Polyeptone	0.3	%	Wako (Cat# 394-00115)
Glucose	5	%	Nacalai Tesque (Cat#16806-25)

Supplement 15 Pre-sporulation medium (Galactose)

Name	Concentration		Manufacture Description
Yeast extract	0.8	%	Nacalai Tesque (Cat# 15838-45)
Polyeptone	0.3	%	Wako (Cat# 394-00115)
Raffinose	7.5	%	Sigma (Cat# R0250)
Galactose	5	%	Sigma (Cat# G0750)

Supplement 16 Sporulation medium

Name	Concentration		Manufacture Description
Potassium acetate	1	%	Nacalai Tesque (Cat# 28404-15)
Uracil	0.002	%	Wako (Cat# 212-00062)
L-Histidine	0.002	%	Wako (Cat# 084-00682)
L-Methionine	0.002	%	Wako (Cat# 133-01602)
L-Leucine	0.003	%	Wako (Cat# 124-00852)
L-Lysine	0.003	%	Wako (Cat# 124-01452)

Supplement 17 LiSorb buffer

Name	Concentration		Manufacture Description
Lithium Acetate (LiOAc)	100	mM	Wako (Cat# 120-01535)
Tris-HCl (pH 8.0)	10	mM	Nacalai Tesque (Cat# 35434-21)
EDTA	1	mM	Nacalai Tesque (Cat# 15105-35)
D-Sorbitol	1	M	Merck (Cat# L580 65059)

Supplement 18 LiPEG buffer

Name	Concentration		Manufacture Description
LiOAc	100	mM	Wako (Cat# 120-01535)
Tris-HCl (pH 8.0)	10	mM	Nacalai Tesque (Cat# 35434-21)
EDTA	1	mM	Nacalai Tesque (Cat# 15105-35)
Polyethylene Glycol (MW~3500 (PEG3350))	40	% (w/v)	Sigma (Cat# P3640-500G)

Supplement 19 Zymolyase buffer

Name	Concentration		Manufacture Description
Zymolyase-20T	0.5	% (w/v)	SEIKAGAKU BIOSCIENCE CORPORATION (Cat# 120491)
D-Sorbitol	1	M	Wako (Cat# 198-03755)
Na_2HPO_4	12.8	mM	Wako (Cat# 196-02835)
NaH_2PO_4	5.6	mM	Wako (Cat# 192-02815)